Distributed Detection in Wireless Sensor Networks under Multiplicative Fading via Generalized Score-tests

Domenico Ciuonzo, *Senior Member, IEEE*, Pierluigi Salvo Rossi, *Senior Member, IEEE* and Pramod K. Varshney, *Life Fellow, IEEE*

***Abstract*—In this paper, we address the problem of distributed detection of a non-cooperative (unknown emitted signal) target with a Wireless Sensor Network (WSN). When the target is present, sensors observe an (unknown) deterministic signal with attenuation depending on the unknown distance between the sensor and the target, multiplicative fading, and additive Gaussian noise. To model energy-constrained operations within Internet of Things (IoT), one-bit sensor measurement quantization is employed and two strategies for quantization are investigated. The Fusion Center (FC) receives sensor bits via noisy Binary Symmetric Channels (BSCs) and provides a more accurate global inference. Such a model leads to a test with nuisances (i.e. the target position x_T) observable only under $\mathcal{H}_1$ hypothesis. Davies' framework is exploited herein to design the generalized forms of Rao and Locally-Optimum Detection (LOD) tests. For our generalized Rao and LOD approaches, a heuristic approach for threshold-optimization is also proposed. Simulation results confirm the promising performance of our proposed approaches.**

***Index Terms*—Distributed detection; Generalized Likelihood Ratio Test; Internet of Things (IoT); Locally-Optimum Detection (LOD), Rao test; Wireless Sensor Networks (WSNs).**

I. Introduction

THE INTERNET OF THINGS (IoT) envisages billions of tiny devices with sensing, computation, and communication capabilities to be used in everyday life and currently represents a game-changing technology for the wireless communications and sensing sector [1], [2]. Wireless Sensor Networks (WSNs) constitute the "sensing arm" of the IoT, with *Distributed Detection* (DD) representing a widely-investigated task [3], [4] having multifold applications such as cognitive radio systems [5], [6] or surveillance [7]. Unfortunately, strict bandwidth and energy constraints in WSNs hamper full-precision reporting by the sensors, which usually are limited to sending one bit to the Fusion Center (FC) regarding the inferred hypothesis. For the mentioned reason, in last years several works have focused on DD based on one-bit quantized measurements [8], [9], [10]. In such a case, the optimal decision procedure at the sensors is one-bit quantization of the local Likelihood-Ratio (LR) [11], [12]. There are two problems with this procedure. First, the design complexity of the quantizer thresholds grows exponentially [13], [14] and, second, the sensor LR cannot be evaluated due to unknown target parameters [14]. Hence, the bit reported is either the outcome of a raw-measurement quantization [15], [16], [17] or represents the inferred binary-valued event (via sub-optimal detection statistics [18]).

In both options, the FC gathers the sensor-generated bits and fuses them via a suitably-designed fusion rule to improve the single-sensor detection capability. In IoT-based systems, the FC could be hosted in the cloud by implementing a "sensing as a service" paradigm [19]. The optimum fusion

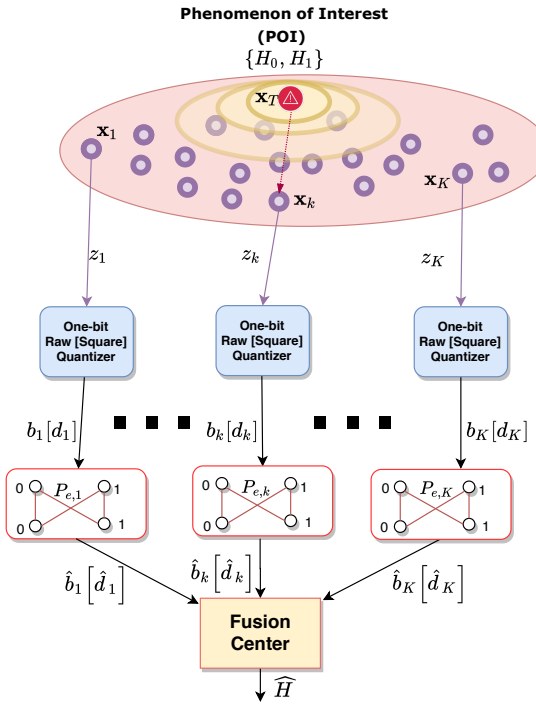

Figure 1: System model considered.

Manuscript received 24th July 2020, revised on 31th December 2020, accepted on 27th January 2021.
This research is a part of BRU21 – NTNU Research and Innovation Program on Digital and Automation Solutions for the Oil and Gas Industry (www.ntnu.edu/bru21).
D. Ciuonzo is with the Department of Electrical Engineering and Information Technologies (DIETI), University of Naples "Federico II", Naples, Italy. E-mail: domenico.ciuonzo@unina.it.
P. Salvo Rossi is with the Department of Electronic Systems, Norwegian University of Science and Technology, Trondheim, Norway and with the Department of Gas Technology, SINTEF Energy Research, Trondheim, Norway. E-mail: salvorossi@ieee.org.
P. K. Varshney is with the Department of Electrical Engineering and Computer Science, Syracuse University, Syracuse, NY 13244, USA. E-mail: varshney@syr.edu.

rule, under conditional independence, involves the comparison of a weighted sum of the received sensor bits with a threshold, with weights depending on the unknown target parameters [3]. Still, when the model is parametrically-specified (with some parameters unknown), the FC faces a composite test of hypotheses and the Generalized LRT (GLRT) is the usual design choice [20]. Indeed, GLRT-based fusion of quantized data has been extensively studied in the DD-focused WSN literature [16], [21], [22], including the challenging case of an unknown source located at an unknown position (*uncooperative target*), because it requires the least amount of knowledge. Accordingly, some recent works have dealt with this problem [15], [22], [7], [23], [24]. In [22], a GLRT was derived for detecting a target with unknown position and emitted power. To obtain computationally simpler solutions (not requiring a grid search over both the target location and the emitted power/signal domains), *generalized* forms of *score tests* (abbreviated as G-Score tests) have been proposed for non-cooperative detection of both *deterministic* [15] and *stochastic* target emissions [7], [23]. Recently, [25] and [24], [26] have addressed the challenging *multiplicative fading* scenario in distributed estimation and detection problems, respectively. The latter scenario is a generalization of both deterministic and stochastic models, and is able to model complicated propagation mechanisms (e.g. a Rician model or estimated small-scale fading).

The *main contributions* of this paper are summarized as follows:

- In this paper, we focus on DD of a non-cooperative target with a spatially-dependent emission (signature), that experiences multiplicative fading. Our DD scenario encompasses detection of a non-cooperative target with an Amplitude Attenuation Function (AAF) depending on the sensor-target distance, one-bit measurement quantization and noisy reporting channels (modelled as Binary Symmetric Channels, BSCs) emulating orthogonal multiple-access channels such as in NB-IoT [27]. Such a scenario encompasses those considered in previous works as special cases [15], [7], [23].
- We consider both Raw Quantization (RQ) and Square-based Quantization (SQ) in the design of low-complexity fusion rules that yield good performance. We show that the usual RQ [26], [24] does not always represent a good choice when non-line-of-sight terms become relevant in multiplicative fading. Hence, we consider SQ to cope with this issue. This operation transforms the composite test from two-sided (on the signal) to one-sided (on the power) with nuisance parameters present only under the hypothesis $\mathcal{H}_1$ [28].
- We *devise* and *optimize* (a) Generalized Rao (G-Rao) and (b) Generalized LOD (G-LOD) approaches based on RQ and SQ, respectively, for the aforementioned scenario. The derived expression is shown to require significantly-lower complexity than their GLR counterparts based on the same quantization type, thus highlighting their practical applicability. Furthermore, the resulting SQ (for G-Rao) and RQ (for G-LOD) optimization (by means of the corresponding quantization thresholds) are shown to be *sensor-individual* (i.e. each threshold can be optimized independently of the others), considers the sensor-FC channel status, and does not depend upon either the target strength or its position, thus allowing *offline* computation.
- A comprehensive simulation-based analysis is presented to compare the proposed G-Rao and G-LOD tests with (i) their GLR counterparts and (ii) tests based on full-precision measurements (i.e. no quantization and reporting loss). The above comparison is performed over relevant WSN parameters, such as the sensing Signal-to-Noise Ratio (SNR), the ratio between direct and scattered terms, and the current reporting channel quality.

We note that the present work extends our earlier conference paper [24] which provided only a *preliminary analysis* of fusion rule design and quantizer optimization based only on the G-Rao test. To the best of our knowledge, only the aforementioned work has tackled DD of an uncooperative target *in the multiplicative fading* case to date.

The remainder of the manuscript is organized as follows. Sec. II states the considered problem; Sec. III develops GLR and G-score tests for the setup introduced; then, Sec. IV focuses on quantizer design; numerical results and concluding discussion are given in Sec. V.

Notation: lower-case bold letters are adopted for vectors, with a_n representing the nth component of $\boldsymbol{a}$; $\mathbb{E}\{\cdot\}$, $(\cdot)^T$ and $u(\cdot)$ denote expectation, vector-transpose and the unit step function, respectively; $p(\cdot)$ and $P(\cdot)$ represent probability density functions (pdf) and probability mass functions (pmf), respectively; χ^2_k (resp. $\chi^{'2}_k(\xi)$) denotes a chi-square (resp. a non-central chi-square) pdf with k degrees of freedom (resp. and non-centrality parameter ξ); $\mathcal{N}(\mu,\sigma^2)$ denotes a Gaussian pdf with mean μ and variance σ^2; $\mathcal{Q}(\cdot)$ (resp. $p_{\mathcal{N}}(\cdot)$) denotes the complementary cumulative distribution function (resp. the pdf) of a normal random variable in its standard form, i.e. $\mathcal{N}(0,1)$; the symbol $\sim$ (resp. $\overset{a}{\sim}$) corresponds to "distributed as" (resp. to "asymptotically distributed as").

II. WSN Model and Problem Formulation

We consider a set of sensors $k \in \mathcal{K} \triangleq \{1,\ldots,K\}$ monitoring a given area to test the absence ($\mathcal{H}_0$) or presence ($\mathcal{H}_1$) of a non-cooperative target. When the target is present ($\mathcal{H}_1$), we assume that it radiates an *unknown deterministic* isotropic signal θ, which is affected by path-loss, multiplicative fading and additive noise, before reaching each sensor:

$$\begin{cases} \mathcal{H}_0: & z_k = w_k \\ \mathcal{H}_1: & z_k = g(\boldsymbol{x}_k,\boldsymbol{x}_T)\, h_k\, \theta + w_k \end{cases}, \tag{1}$$

In Eq. (1), $z_k \in \mathbb{R}$ denotes the kth sensor observation, whereas $w_k \sim \mathcal{N}(0,\sigma^2_{w,k})$ and $h_k \sim \mathcal{N}(\mu_{h,k},\sigma^2_{h,k})$ are the noise and multiplicative fading terms, respectively[1]. Also, $\boldsymbol{x}_k \in \mathbb{R}^d$ denotes the *known* kth sensor position (obtained via self-localization procedures), while $\boldsymbol{x}_T \in \mathbb{R}^d$ denotes the *unknown* target position. Both the terms $\boldsymbol{x}_T$ and $\boldsymbol{x}_k$ determine

[1]We hypothesize that sufficient spatial separation of the sensors implies statistical independence of noise and fading terms w_ks and h_ks.

the value of the *generic* Amplitude Attenuation Function (AAF) $g(\boldsymbol{x}_T, \boldsymbol{x}_k)$. In fact, any functional form of the AAF (accounting for the spatial target signature) may be considered in this paper, given the availability of $g(\cdot,\cdot)$ at the FC[2].

For compactness, in what follows, we use the shorthand notation $g_k \triangleq g(\boldsymbol{x}_T, \boldsymbol{x}_k)$. Hence, based on the above assumptions, $z_k|\mathcal{H}_0 \sim \mathcal{N}(0, \sigma^2_{w,k})$ and $z_k|\mathcal{H}_1 \sim \mathcal{N}(g_k\,\mu_{h,k}\,\theta\,,\,\sigma^2_{\mathrm{eq},k}(\theta))$, $k \in \mathcal{K}$, where $\sigma^2_{\mathrm{eq},k}(\theta) = (g_k^2\,\sigma^2_{h,k}\,\theta^2 + \sigma^2_{w,k})$ denotes the kth *equivalent variance*.

Furthermore, we define the (a) target Signal-To-Noise Ratio (SNR) and (b) the ratio between direct (Line-of-Sight, LoS) and scattered (Non Line-of-Sight, NLoS) target power terms respectively as

$$\mathrm{SNR} \triangleq 10\,\log_{10}(\theta^2\,(\mu_h^2+\sigma_h^2)\,/\sigma_w^2) \quad (2)$$

$$\kappa \triangleq 10\,\log_{10}(\mu_h^2\,/\sigma_h^2) \quad (3)$$

To address the energy and bandwidth limitations in IoT scenarios, the kth sensor quantizes z_k into a single bit[3]. Herein, we investigate *two* quantization strategies. In the first case, we consider the usual *Raw Quantization* (RQ) [15], namely $b_k \triangleq u\,(z_k - \tau_k)$. In the second case, we investigate *Square-based Quantizers* (SQ), namely $d_k \triangleq u(z_k^2 - \gamma_k)$, which was used for the purely-random (viz. stochastic) signal case in [23], [29]. For RQ, the bit detection probability under $\mathcal{H}_1$ equals

$$\beta_k(\theta, \boldsymbol{x}_T) \triangleq \mathcal{Q}\left([\tau_k - g_k\,\mu_{h,k}\,\theta]\,/\,\sqrt{\sigma^2_{\mathrm{eq},k}(\theta)}\right), \quad (4)$$

while for $\mathcal{H}_0$ it is given by $\beta_{0,k} \triangleq \beta_k(\theta = 0, \boldsymbol{x}_T) = \mathcal{Q}(\tau_k/\sqrt{\sigma^2_{w,k}})$. Differently, for SQ, the bit detection probability under $\mathcal{H}_1$ equals

$$\rho_k(\theta, \boldsymbol{x}_T) \triangleq \mathcal{Q}\left([\sqrt{\gamma_k} - g_k\,\mu_{h,k}\,\theta]\,/\,\sqrt{\sigma^2_{\mathrm{eq},k}(\theta)}\right) + \mathcal{Q}\left([\sqrt{\gamma_k} + g_k\,\mu_{h,k}\,\theta]\,/\,\sqrt{\sigma^2_{\mathrm{eq},k}(\theta)}\right), \quad (5)$$

while for $\mathcal{H}_0$ it is $\rho_{0,k} \triangleq \rho_k(\theta = 0, \boldsymbol{x}_T) = 2\,\mathcal{Q}\left(\sqrt{\gamma_k/\sigma^2_{w,k}}\right)$.

To model energy-constrained communications within the IoT context, after RQ (resp. SQ) the kth sensor bit b_k (resp. d_k) is sent over a channel modeled as a BSC. Hence, the FC receives a noisy version $\hat{b}_k$ (resp. $\hat{d}_k$), where $P_{\mathrm{e},k}$ denotes the *known* bit-error probability of the kth link, namely $\hat{b}_k = (1 - b_k)$ (resp. $\hat{d}_k = (1 - d_k)$) with bit-flip probability $P_{\mathrm{e},k}$. We note that the considered set of independent BSCs can emulate the modulation-decoding process[4] usually adopted in WSNs and IoT applications employing the uplink of the narrowband IoT (NB-IoT) standard [27]. Indeed, although WSNs need to provide connectivity to a large number of sensors, the latter have low data rate requirements. Accordingly, low-order modulation schemes (e.g. BPSK) and single-carrier frequency division multiple access perfectly fit their needs. Such configuration is a common operational mode of NB-IoT uplink, as detailed in what follows.

More specifically, NB-IoT has a bandwidth of $180\,\mathrm{kHz}$, corresponding to one LTE physical resource block. Additionally, a possible subcarrier spacing equals $3.75\,\mathrm{kHz}$ (the other configuration spacing allowed is $15\,\mathrm{kHz}$) in single-tone transmission, for a total of 48 subcarriers, and each subcarrier can be allocated to a different user for a time slot of $32\,\mathrm{ms}$. The latter constitutes the elementary *resource unit to be allocated to a single user for sending its data.* Therefore, if the sensing duty cycle for each node is $0.1\,\mathrm{s}$, then the system can support the non-interfering transmission/reception of more than 150 sensors performing one-bit quantization of their corresponding measurements in a given cell. In view of these considerations, we can safely hypothesize orthogonal channels between the sensors and the FC, similar to [2].

For the sake of a compact notation, we collect the received bits as $\widehat{\boldsymbol{b}} \triangleq \left[\begin{array}{ccc}\hat{b}_1 & \cdots & \hat{b}_K\end{array}\right]^T$ and $\widehat{\boldsymbol{d}} \triangleq \left[\begin{array}{ccc}\hat{d}_1 & \cdots & \hat{d}_K\end{array}\right]^T$ in RQ and SQ cases, respectively.

Given these assumptions, when RQ is applied, the probability that $\hat{b}_k = 1$ under $\mathcal{H}_1$ is given by $\alpha_k^{\mathrm{rq}}(\theta, \boldsymbol{x}_T) \triangleq (1 - P_{e,k})\beta_k(\theta, \boldsymbol{x}_T) + P_{e,k}(1 - \beta_k(\theta, \boldsymbol{x}_T))$, whereas under $\mathcal{H}_0$ $\alpha_{0,k}^{\mathrm{rq}} = (1 - P_{e,k})\beta_{0,k} + P_{e,k}(1 - \beta_{0,k})$. Similarly, when SQ is adopted, the probability that $\hat{d}_k = 1$ under $\mathcal{H}_1$ is given by $\alpha_k^{\mathrm{sq}}(\theta, \boldsymbol{x}_T) \triangleq (1 - P_{e,k})\rho_k(\theta, \boldsymbol{x}_T) + P_{e,k}(1 - \rho_k(\theta, \boldsymbol{x}_T))$, whereas under $\mathcal{H}_0$ the expression equals $\alpha_{0,k}^{\mathrm{sq}} = (1 - P_{e,k})\rho_{0,k} + P_{e,k}(1 - \rho_{0,k})$.

Definition of Test of Hypotheses: Note that the full-precision testing problem, i.e., that assumes the availability of original measurements $z_1, \ldots z_K$, depends on the unknown target position $\boldsymbol{x}_T$, which can be observed at the FC *only* when the *signal is present* ($\theta \neq \theta_0$, where $\theta_0 = 0$), i.e. $\{\mathcal{H}_0, \mathcal{H}_1\} \rightarrow \{\theta = \theta_0, \theta \neq \theta_0\}$. Hence, the test with full-precision measurements is a two-sided one with a nuisance term ($\boldsymbol{x}_T$) identifiable only under $\mathcal{H}_1$ [28].

However, when considering the two quantization approaches, some *further clarifications* are necessary. In the case of RQ, the unknown target position $\boldsymbol{x}_T$ can be observed at the FC *only* when the *signal is present* ($\theta \neq \theta_0$, where $\theta_0 = 0$), i.e. $\{\mathcal{H}_0, \mathcal{H}_1\} \rightarrow \{\theta = \theta_0, \theta \neq \theta_0\}$, since $\beta_k(\theta, \boldsymbol{x}_T)$ (and, as a consequence, $\alpha_k^{\mathrm{rq}}(\theta, \boldsymbol{x}_T)$) depends on θ. Hence, the corresponding test is again a two-sided one with a nuisance term ($\boldsymbol{x}_T$) identifiable only under $\mathcal{H}_1$ [28]. Conversely, when considering SQ, the kth probability $\rho_k(\theta, \boldsymbol{x}_T)$ (and, as a

[2]The latter functional form may be estimated by means of some *training data* obtained by running an initialization phase (consisting of $n = 1, \ldots, N$ timeslots) in which a *cooperative* target (with emitted signal $\theta[n]$ and position $\boldsymbol{x}_T[n]$ *known* at the FC) moves throughout the surveilled area and the (quantized) measurements transmitted by the WSN are collected by the FC. Once a sufficient number of training data has been gathered, the AAF may be estimated via standard learning techniques (e.g. kernel-based regression).

[3]In this work we restrict our attention to (i) deterministic and (ii) one-bit quantizers. Still, the proposed fusion methodology (including the quantizer optimization later reported in Sec. IV) could be in principle applied also in the general case of non-deterministic (e.g. dithered) and multi-bit quantizers. The above interesting generalization is however left to future studies.

[4]We remark that the explicit inclusion of noisy and fading effects in the model underlying the design of the presented fusion rules (that is, considering a "decode-and-fuse" approach [30]), although promising in terms of achievable performance gains, constitutes a challenging task. This is due to the more involved expression of the pdf of the resulting received signal vector and to the difficulty in the evaluation of the consequent score/FI expressions. For this reason, the design of aforementioned class of fusion rules is left to future studies.

consequence, $\alpha_k^{\mathrm{sq}}(\theta, \boldsymbol{x}_T))$ is actually a function of the target emitted power $P_\theta \triangleq \theta^2$. Therefore, we have:

$$\rho_k(P_\theta, \boldsymbol{x}_T) \triangleq \mathcal{Q}\left(\left[\sqrt{\gamma_k} - |g_k\, \mu_{h,k}|\, \sqrt{P_\theta}\right] / \sqrt{\sigma^2_{\mathrm{eq},k}(P_\theta)} \right) + \mathcal{Q}\left(\left[\sqrt{\gamma_k} + |g_k\, \mu_{h,k}|\, \sqrt{P_\theta}\right] / \sqrt{\sigma^2_{\mathrm{eq},k}(P_\theta)} \right), \tag{6}$$

where $\sigma^2_{\mathrm{eq},k}(P_\theta) = (g_k^2\, \sigma^2_{h,k}\, P_\theta + \sigma^2_{w,k})$. Hence $\boldsymbol{x}_T$ can be observed *only* when the *power is present* ($P_\theta > P_{\theta_0}$, where $P_{\theta_0} = 0$), i.e. $\{\mathcal{H}_0, \mathcal{H}_1\} \rightarrow \{P_\theta = P_{\theta_0}, P_\theta > P_{\theta_0}\}$. Thus, in the SQ case, we test a one-sided parameter with a nuisance term ($\boldsymbol{x}_T$) identifiable only under $\mathcal{H}_1$ [28].

The aim of our study is to design a simple test (from a computational viewpoint) deciding in favor of $\mathcal{H}_0$ (resp. $\mathcal{H}_1$) when the statistic ($\Lambda(\hat{\boldsymbol{b}})$ or $\Lambda(\hat{\boldsymbol{d}})$) is below (resp. above) the threshold γ_{fc}, and the design of the quantizer (i.e. optimized τ_k or γ_k, $k \in \mathcal{K}$) for each sensor. The FC performance is evaluated in terms of its false alarm ($P_{\mathrm{F}} \triangleq \Pr\{\Lambda > \gamma_{\mathrm{fc}} | \mathcal{H}_0\}$) and detection ($P_{\mathrm{D}} \triangleq \Pr\{\Lambda > \gamma_{\mathrm{fc}} | \mathcal{H}_1\}$) probabilities, respectively, with Λ denoting the generic decision statistic at the FC.

III. Design of the Fusion Rules

First of all, we observe that the log-likelihood function of the received vector $\hat{\boldsymbol{b}}$ versus $(\theta, \boldsymbol{x}_T)$, namely $\log P(\hat{\boldsymbol{b}}; \theta, \boldsymbol{x}_T)$, can be expressed in explicit form as [7], [22]

$$\sum_{k=1}^{K} \{\hat{b}_k \log[\alpha_k^{\mathrm{rq}}(\theta, \boldsymbol{x}_T)] + (1 - \hat{b}_k) \log[1 - \alpha_k^{\mathrm{rq}}(\theta, \boldsymbol{x}_T)]\}. \tag{7}$$

We recall that the above expression holds also for SQ, i.e., with the log-likelihood $\log P(\hat{\boldsymbol{d}}; \theta, \boldsymbol{x}_T)$, if we replace $\hat{b}_k$ and $\alpha_k^{\mathrm{rq}}(\theta, \boldsymbol{x}_T)$ with $\hat{d}_k$ and $\alpha_k^{\mathrm{sq}}(\theta, \boldsymbol{x}_T)$, respectively. We now introduce the design rationales considered for obtaining the proposed fusion rules.

The GLR is the most common approach for tests with composite hypotheses [22], with its implicit expression for the decision statistic based on RQ given by

$$\Lambda_{\mathrm{GLR}}(\hat{\boldsymbol{b}}) \triangleq 2 \log \left[\frac{P(\hat{\boldsymbol{b}}; \hat{\theta}_1, \widehat{\boldsymbol{x}}_T)}{P(\hat{\boldsymbol{b}}; \theta_0)} \right]. \tag{8}$$

In the above equation, the pair $(\hat{\theta}_1, \widehat{\boldsymbol{x}}_T)$ represents the *Maximum Likelihood* (ML) *estimates* under $\mathcal{H}_1$, i.e.

$$(\hat{\theta}_1, \widehat{\boldsymbol{x}}_T) \triangleq \arg \max_{(\theta, \boldsymbol{x}_T)} P(\hat{\boldsymbol{b}}; \theta, \boldsymbol{x}_T). \tag{9}$$

Similarly, the GLR statistic based on SQ is given by

$$\Lambda_{\mathrm{GLR}}(\hat{\boldsymbol{d}}) \triangleq 2 \log \left[\frac{P(\hat{\boldsymbol{d}}; \hat{P}_{\theta_1}, \widehat{\boldsymbol{x}}_T)}{P(\hat{\boldsymbol{d}}; P_{\theta_0})} \right]. \tag{10}$$

Analogously, the pair $(\hat{P}_{\theta_1}, \widehat{\boldsymbol{x}}_T)$ represents the ML *estimates* under $\mathcal{H}_1$, obtained as

$$(\hat{P}_{\theta_1}, \widehat{\boldsymbol{x}}_T) \triangleq \arg \max_{(P_\theta, \boldsymbol{x}_T)} P(\hat{\boldsymbol{d}}; P_\theta, \boldsymbol{x}_T). \tag{11}$$

We observe that Λ_{GLR} (see Eqs. (8) and (10)) requires the solution of an optimization task. Unfortunately, the ML estimate pair $(\hat{\theta}_1, \widehat{\boldsymbol{x}}_T)$ (resp. $(\hat{P}_{\theta_1}, \widehat{\boldsymbol{x}}_T)$) cannot be obtained in closed form and this hinders its practical implementation. Hence, a (joint) grid approach is usually adopted on $(\theta, \boldsymbol{x}_T)$ (resp. $(P_\theta, \boldsymbol{x}_T)$) [7], [21], [22]. Accordingly, the GLR statistic is able to provide an estimate for *both* the emitted signal θ (resp. power P_θ) and the target location $\boldsymbol{x}_T$.

On the other hand, Davies' work represents an alternative approach for capitalizing on either the two-sided (when RQ is applied) or one-sided (when SQ is applied) nature of the considered hypothesis test [28], allowing to generalize score tests to the more challenging scenario of nuisance parameters observed *only* under $\mathcal{H}_1$. In fact, score tests rely on the ML estimates of nuisances under $\mathcal{H}_0$ [20], that cannot be obtained here since they are *unobservable*.

For instance, referring to our model and considering the design of a Rao test (based on RQ), the numerator of the statistics would be given by $(\partial \log \left[P\left(\hat{\boldsymbol{b}}; \theta, \boldsymbol{x}_T\right) \right] / \partial \theta)^2 \Big|_{\theta=\theta_0,\, \boldsymbol{x}_T = \hat{\boldsymbol{x}}_{T,0}}$, where $\hat{\boldsymbol{x}}_{T,0}$ represents the ML estimate of the target position under $\mathcal{H}_0$. However, when the hypothesis $\mathcal{H}_0$ holds, the target is *absent* and thus its position $\boldsymbol{x}_T$ *cannot be estimated*.

Conversely, if $\boldsymbol{x}_T$ were known, the Rao (LOD) statistic would represent a suitable decision statistic for the corresponding two-sided (resp. one-sided) testing on θ (resp. P_θ) [20]. Unfortunately, since the target location parameter is not known in our case, we rather obtain a functional score statistics *indexed* by $\boldsymbol{x}_T$. Thus, to overcome this technical difficulty, Davies proposed the *functional supremum* as the relevant statistic, that is:

$$\Lambda_{\mathrm{GRao}}\left(\widehat{\boldsymbol{b}}\right) \triangleq \max_{\boldsymbol{x}_T} \frac{\left(\partial \log \left[P\left(\hat{\boldsymbol{b}}; \theta, \boldsymbol{x}_T\right) \right] / \partial \theta \right)^2 \Big|_{\theta=\theta_0}}{\mathrm{I}^{\mathrm{rq}}(\theta_0, \boldsymbol{x}_T)} \tag{12}$$

$$\Lambda_{\mathrm{GLOD}}\left(\widehat{\boldsymbol{d}}\right) \triangleq \max_{\boldsymbol{x}_T} \frac{\partial \log \left[P\left(\hat{\boldsymbol{d}}; P_\theta, \boldsymbol{x}_T\right) \right] / \partial P_\theta \Big|_{P_\theta = P_{\theta_0}}}{\sqrt{I^{\mathrm{sq}}(P_{\theta_0}, \boldsymbol{x}_T)}} \tag{13}$$

where $I^{\mathrm{rq}}(\theta, \boldsymbol{x}_T) \triangleq \mathbb{E}\left\{ \left(\partial \log[P(\hat{\boldsymbol{b}}; \theta, \boldsymbol{x}_T)] / \partial \theta \right)^2 \right\}$ represents the Fisher Information (FI) of $\hat{\boldsymbol{b}}$ (with respect to θ), assuming $\boldsymbol{x}_T$ *known*. Similarly, $I^{\mathrm{sq}}(P_\theta, \boldsymbol{x}_T) \triangleq \mathbb{E}\left\{ \left(\partial [\log(\hat{\boldsymbol{d}}; P_\theta, \boldsymbol{x}_T)] / \partial P_\theta \right)^2 \right\}$ represents the Fisher Information (FI) of $\hat{\boldsymbol{d}}$ (with respect to P_θ), assuming $\boldsymbol{x}_T$ *known.* The underlying idea of Davies' approach is to select a test which accepts the hypothesis $\mathcal{H}_1$ when the functional statistic evaluated at the most-likely target position (i.e. that corresponding to $\arg\max_{\boldsymbol{x}_T} \Lambda(\cdot; \boldsymbol{x}_T)$) exceeds a given threshold γ_{fc}. This choice can be also interpreted as a "GLRT-like" philosophy on these particular nuisance parameters. Accordingly, both the generalized score statistics in Eqs. (12) and (13) implicitly estimate *only* the target location $\boldsymbol{x}_T$.

Hereinafter, we will refer to the decision statistics in Eqs. (12) and (13) as *Generalized Rao* (G-Rao) and *Generalized LOD* (G-LOD)*, respectively,* to indicate the use of Rao and LOD as the inner statistic within Davies framework [7].

The closed-form expression of Λ_{GRao} is drawn by means of the explicit forms of the score function (i.e.

$\partial \log[P(\widehat{\boldsymbol{b}};\theta,\boldsymbol{x}_T)/\partial\theta])$ and the FI (i.e. $\mathrm{I}^{\mathrm{rq}}(\theta,\boldsymbol{x}_T)$), *both evaluated* at $\theta=\theta_0$. Their derivation is provided in Appendices A and B, respectively. In the former case, the final expression of the ($\boldsymbol{x}_T$-conditional) score function at $\theta=\theta_0$ is given by

$$\left.\frac{\partial \log P(\hat{\boldsymbol{b}};\theta,\boldsymbol{x}_T)}{\partial\theta}\right|_{\theta=\theta_0} = \sum_{k=1}^{K}\left(\hat{b}_k-\alpha_{0,k}^{\mathrm{rq}}\right)\Xi_k^{\mathrm{rq}}\,g_k\,, \quad (14)$$

where the auxiliary definition

$$\Xi_k^{\mathrm{rq}} \triangleq \frac{(1-2P_{\mathrm{e},k})}{\alpha_{0,k}^{\mathrm{rq}}\left[1-\alpha_{0,k}^{\mathrm{rq}}\right]}\frac{\mu_{h,k}}{\sigma_{w,k}}\,p_{\mathcal{N}}\left(\frac{\tau_k}{\sqrt{\sigma_{w,k}^2}}\right) \quad (15)$$

has been employed. We recall that $p_{\mathcal{N}}(\cdot)$ is used to denote the pdf of a normal random variable in its standard form. Also, we highlight that the term Ξ_k^{rq} allows to express the ($\boldsymbol{x}_T$-conditional) score function at $\theta=\theta_0$ in Eq. (14) in a compact form by separating deterministic terms not depending on $\boldsymbol{x}_T$ from (a) random contributions (i.e. $(\hat{b}_k-\alpha_{0,k}^{\mathrm{rq}})$) and ($b$) deterministic terms which are instead function of $\boldsymbol{x}_T$ (i.e. g_k). In the latter case, the ($\boldsymbol{x}_T$-conditional) FI at θ_0 is given by

$$\begin{aligned} I^{\mathrm{rq}}(\theta_0,\boldsymbol{x}_T) &= \sum_{k=1}^{K}\alpha_{0,k}^{\mathrm{rq}}(1-\alpha_{0,k}^{\mathrm{rq}})\,(\Xi_k^{\mathrm{rq}})^2\,g_k^2 \\ &= \sum_{k=1}^{K}\psi_{0,k}^{\mathrm{rq}}\,g_k^2 \end{aligned} \quad (16)$$

where the definition $\psi_{0,k}^{\mathrm{rq}} \triangleq \alpha_{0,k}^{\mathrm{rq}}(1-\alpha_{0,k}^{\mathrm{rq}})\,(\Xi_k^{\mathrm{rq}})^2$ has been employed in the last line. Accordingly, the explicit form of the G-Rao statistic can be thus rewritten as $\Lambda_{\mathrm{GRao}}(\widehat{\boldsymbol{b}}) \triangleq \max_{\boldsymbol{x}_T}\Lambda_{\mathrm{Rao}}(\widehat{\boldsymbol{b}},\boldsymbol{x}_T)$, where

$$\Lambda_{\mathrm{Rao}}\left(\widehat{\boldsymbol{b}},\boldsymbol{x}_T\right) = \frac{\left\{\sum_{k=1}^{K}\nu_k^{\mathrm{rq}}(\widehat{b}_k)\,g(\boldsymbol{x}_T,\boldsymbol{x}_k)\right\}^2}{\sum_{k=1}^{K}\psi_{0,k}^{\mathrm{rq}}\,g^2(\boldsymbol{x}_T,\boldsymbol{x}_k)} \quad (17)$$

denotes the Rao statistic assuming $\boldsymbol{x}_T$ known, and we have defined $\nu_k^{\mathrm{rq}}(\widehat{b}_k) \triangleq (\widehat{b}_k-\alpha_{0,k}^{\mathrm{rq}})\,\Xi_k^{\mathrm{rq}}$.

In contrast, the explicit expression of Λ_{GLOD} is drawn by means of the explicit forms of the score function $(\log\left[P\left(\widehat{\boldsymbol{d}};P_\theta,\boldsymbol{x}_T\right)\right]/\partial P_\theta)$ and the FI ($I^{\mathrm{sq}}(P_\theta,\boldsymbol{x}_T)$), *both evaluated* at $P_\theta=P_{\theta_0}$. Their derivation is provided in the Appendices A and B, respectively. In the former case, the final expression of the ($\boldsymbol{x}_T$-conditional) score function at $P_\theta=P_{\theta_0}$ is given by:

$$\left.\frac{\partial \log P(\hat{\boldsymbol{d}};\theta,\boldsymbol{x}_T)}{\partial P_\theta}\right|_{P_\theta=P_{\theta_0}} = \sum_{k=1}^{K}\left(\hat{d}_k-\alpha_{0,k}^{\mathrm{sq}}\right)\Xi_k^{\mathrm{sq}}\,g_k^2 \quad (18)$$

where the definition

$$\Xi_k^{\mathrm{sq}} \triangleq \frac{(1-2P_{\mathrm{e},k})\,\sqrt{\gamma_k}\,(\mu_{h,k}^2+\sigma_{h,k}^2)}{\alpha_{0,k}^{\mathrm{sq}}\left[1-\alpha_{0,k}^{\mathrm{sq}}\right]\,\sigma_{w,k}^3}\,p_{\mathcal{N}}\left(\sqrt{\frac{\gamma_k}{\sigma_{w,k}^2}}\right) \quad (19)$$

has been employed. We highlight that the term Ξ_k^{sq} allows to express the ($\boldsymbol{x}_T$-conditional) score function at $P_\theta=P_{\theta_0}$ in Eq. (18) in a compact form by separating deterministic terms not depending on $\boldsymbol{x}_T$ from (a) random contributions (i.e. $(\hat{d}_k-\alpha_{0,k}^{\mathrm{sq}})$) and ($b$) deterministic terms which are instead function of $\boldsymbol{x}_T$ (i.e. g_k^2). In the latter case, the ($\boldsymbol{x}_T$-conditional) FI at P_{θ_0} is given by

$$\begin{aligned} I^{\mathrm{sq}}(P_{\theta_0},\boldsymbol{x}_T) &= \sum_{k=1}^{K}\alpha_{0,k}^{\mathrm{sq}}\,(1-\alpha_{0,k}^{\mathrm{sq}})\,(\Xi_k^{\mathrm{sq}})^2\,g_k^4 \\ &= \sum_{k=1}^{K}\psi_{0,k}^{\mathrm{sq}}\,g_k^4 \end{aligned} \quad (20)$$

where the definition $\psi_{0,k}^{\mathrm{sq}} \triangleq \alpha_{0,k}^{\mathrm{sq}}\left(1-\alpha_{0,k}^{\mathrm{sq}}\right)(\Xi_k^{\mathrm{sq}})^2$ has been employed in the last line. As a result, the explicit form of the G-LOD statistic can be shown to be $\Lambda_{\mathrm{GLOD}}(\widehat{\boldsymbol{d}}) \triangleq \max_{\boldsymbol{x}_T}\Lambda_{\mathrm{LOD}}(\widehat{\boldsymbol{d}},\boldsymbol{x}_T)$, where

$$\Lambda_{\mathrm{LOD}}\left(\widehat{\boldsymbol{d}},\boldsymbol{x}_T\right) = \frac{\sum_{k=1}^{K}\nu_k^{\mathrm{sq}}(\widehat{d}_k)\,g^2(\boldsymbol{x}_T,\boldsymbol{x}_k)}{\sqrt{\sum_{k=1}^{K}\psi_{0,k}^{\mathrm{sq}}\,g^4(\boldsymbol{x}_T,\boldsymbol{x}_k)}} \quad (21)$$

denotes the LOD statistic assuming $\boldsymbol{x}_T$ known, and we have defined $\nu_k^{\mathrm{sq}}(\widehat{d}_k) \triangleq (\widehat{d}_k-\alpha_{0,k}^{\mathrm{sq}})\,\Xi_k^{\mathrm{sq}}$.

The appeal of G-Rao and G-LOD statistics is motivated by their *simpler implementation* (as $\hat{\theta}_1$ and $P_{\hat{\theta}_1}$ are not needed), requiring solely a grid with respect to $\boldsymbol{x}_T$, that is

$$\Lambda_{\mathrm{GRao}}(\widehat{\boldsymbol{b}}) \approx \max_{i=1,\ldots N_{\boldsymbol{x}_T}}\Lambda_{\mathrm{Rao}}(\widehat{\boldsymbol{b}},\boldsymbol{x}_T[i]) \quad (22)$$

$$\Lambda_{\mathrm{GLOD}}(\widehat{\boldsymbol{d}}) \approx \max_{i=1,\ldots N_{\boldsymbol{x}_T}}\Lambda_{\mathrm{LOD}}(\widehat{\boldsymbol{d}},\boldsymbol{x}_T[i]) \quad (23)$$

Thus, their complexity is $\mathcal{O}(K\,N_{\boldsymbol{x}_T})$, implying a *significant reduction* with respect to the GLR. Indeed, the complexity of the latter equals $\mathcal{O}(K\,N_{\boldsymbol{x}_T}\,N_\theta)$ and $\mathcal{O}(K\,N_{\boldsymbol{x}_T}\,N_{P_\theta})$ when RQ and SQ are adopted, respectively. In the above expressions, the terms $N_{\boldsymbol{x}_T}$ and N_θ (resp. N_{P_θ}) denote the number of position and amplitude (resp. power) bins employed. A comparison of the complexity involved in the implementation of the above fusion rules is summarized in Table I.

It is evident that Λ_{GRao} depends on τ_k's (collected as $\boldsymbol{\tau} \triangleq \begin{bmatrix}\tau_1 & \cdots & \tau_K\end{bmatrix}^T$), via the terms $\nu_k^{\mathrm{rq}}(\widehat{b}_k)$ and $\psi_{0,k}^{\mathrm{rq}}$, $k\in\mathcal{K}$, which can be *optimized* to boost performance, as performed in [24]. The same reasoning applies to Λ_{GLOD}, as it is a function of γ_k's (collected as $\boldsymbol{\gamma} \triangleq \begin{bmatrix}\gamma_1 & \cdots & \gamma_K\end{bmatrix}^T$), through $\nu_k^{\mathrm{sq}}(\widehat{d}_k)$ and $\psi_{0,k}^{\mathrm{sq}}$, $k\in\mathcal{K}$, which can be *optimized* as well. We notice that the same optimization applies also to Λ_{GLR} for RQ and SQ cases. We accomplish this objective in what follows.

IV. Optimization of Quantizers Thresholds

We point out that (asymptotically) optimal deterministic quantizers cannot be obtained, since no closed-form performance expressions exist for the tests based on Davies approach [28]. Hence, the rationale in [16], [29], [31] cannot be applied to our case. Due to this reason, we use a modified approach (that resorts to a heuristic, yet intuitive, basis) that has been successfully applied to DD problems for the special cases of either purely deterministic or stochastic target emission [15], [23].

Table I: Summary of fusion rules considered in this work. For each of these, the computational complexity required needed for its implementation (via grid discretization) is also reported (last column).

Fusion Rule	**Quantization**	**Expression**	**Complexity**
GLR$^{\rm rq}$	RQ	$2\,\max_{(\boldsymbol{x}_T,\theta)}\,\sum_{k=1}^{K}\widehat{b}_k\,\log\left[\frac{\alpha_k^{\rm rq}(\theta,\boldsymbol{x}_T)}{\alpha_{0,k}^{\rm rq}}\right]+(1-\widehat{b}_k)\,\log\left[\frac{1-\alpha_k^{\rm rq}(\theta,\boldsymbol{x}_T)}{1-\alpha_{0,k}^{\rm rq}}\right]$	$\mathcal{O}\left(K\,N_{\boldsymbol{x}_T}\,N_\theta\right)$
G-Rao$^{\rm rq}$	RQ	$\max_{\boldsymbol{x}_T}\left\{\sum_{k=1}^{K}\nu_k^{\rm rq}(\widehat{b}_k)\,g_k\right\}^2\,/\,\sum_{k=1}^{K}\psi_{0,k}^{\rm rq}\,g_k^2$	$\mathcal{O}\left(K\,N_{\boldsymbol{x}_T}\right)$
GLR$^{\rm sq}$	SQ	$2\,\max_{(\boldsymbol{x}_T,P_\theta)}\,\sum_{k=1}^{K}\widehat{d}_k\,\log\left[\frac{\alpha_k^{\rm sq}(P_\theta,\boldsymbol{x}_T)}{\alpha_{0,k}^{\rm sq}}\right]+(1-\widehat{d}_k)\,\log\left[\frac{1-\alpha_k^{\rm sq}(P_\theta,\boldsymbol{x}_T)}{1-\alpha_{0,k}^{\rm sq}}\right]$	$\mathcal{O}\left(K\,N_{\boldsymbol{x}_T}\,N_{P_\theta}\right)$
G-LOD$^{\rm sq}$	SQ	$\max_{\boldsymbol{x}_T}\,\sum_{k=1}^{K}\nu_k^{\rm sq}(\widehat{d}_k)\,g_k^2\,/\,\sqrt{\sum_{k=1}^{K}\psi_{0,k}^{\rm sq}\,g_k^4}$	$\mathcal{O}\left(K\,N_{\boldsymbol{x}_T}\right)$
GLR$^{\rm fp}$	–	$\max_{(\boldsymbol{x}_T,\theta)}\,\sum_{k=1}^{K}\log\left[\sigma_{w,k}^2\,/\,\sigma_{{\rm eq},k}^2(\theta)\right]+\left[z_k^2\,/\,\sigma_{{\rm eq},k}^2(\theta)\right]-\left[(z_k-g_k\,\mu_{h,k}\,\theta)^2\,/\,\sigma_{{\rm eq},k}^2(\theta)\right]$	$\mathcal{O}\left(K\,N_{\boldsymbol{x}_T}\,N_\theta\right)$
G-Rao$^{\rm fp}$	–	$\max_{\boldsymbol{x}_T}\,(\sum_{k=1}^{K}g_k\,\mu_{h,k}\,z_k/\sigma_{w,k}^2)^2\,/\,\sum_{k=1}^{K}g_k^2\,\mu_{h,k}^2\,/\,\sigma_{w,k}^2$	$\mathcal{O}\left(K\,N_{\boldsymbol{x}_T}\right)$
G-LOD$^{\rm fp}$	–	$\max_{\boldsymbol{x}_T}\,\sum_{k=1}^{K}\frac{1}{2}\left[\frac{g_k^2}{\sigma_{w,k}^2}(\mu_{h,k}^2+\sigma_{h,k}^2)\left(\frac{z_k^2}{\sigma_{w,k}^2}-1\right)\right]\,/\,\sqrt{\frac{1}{2}\sum_{k=1}^{K}\frac{g_k^4}{\sigma_{w,k}^4}(\mu_{h,k}^2+\sigma_{h,k}^2)^2}$	$\mathcal{O}\left(K\,N_{\boldsymbol{x}_T}\right)$

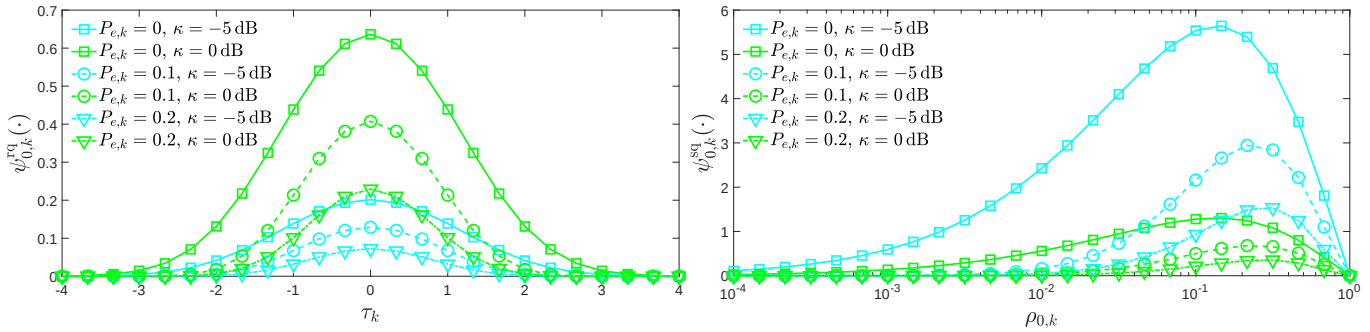

(a) Objective function for selection of $\tau_k^\star$ in G-Rao$^{\rm rq}$ and GLR$^{\rm rq}$.

(b) Objective function for selection of $\rho_{0,k}^\star$ (viz. $\gamma_k^\star$) in G-LOD$^{\rm sq}$ and GLR$^{\rm sq}$.

Figure 2: Threshold objectives used for optimizing RQ ($\psi_{0,k}^{\rm rq}(\tau_k)$, subfigure a) and SQ ($\psi_{0,k}^{\rm sq}(\rho_{0,k})$, subfigure b) for $P_{e,k}\in\{0,0.1,0.2\}$ and $\kappa\in\{-5,0\}$ dB.

In detail, it is well known that the $\boldsymbol{x}_T$-clairvoyant Rao statistic $\Lambda_{\rm Rao}$ is distributed (under an asymptotic, weak-signal, assumption[5]) as [20]

$$\Lambda_{\rm Rao}(\boldsymbol{x}_T,\boldsymbol{\tau})\overset{a}{\sim}\begin{cases}\chi_1^2 & \text{under}\quad\mathcal{H}_0\\ \chi_1'^2\left(\lambda_Q(\boldsymbol{x}_T,\boldsymbol{\tau})\right) & \text{under}\quad\mathcal{H}_1\end{cases},\tag{24}$$

A similar result applies to the $\boldsymbol{x}_T$-clairvoyant LOD statistic $\Lambda_{\rm LOD}$, which is asymptotically (under the same conditions as the Rao test) distributed as [20]

$$\Lambda_{\rm LOD}(\boldsymbol{x}_T,\boldsymbol{\gamma})\overset{a}{\sim}\begin{cases}\mathcal{N}(0,1) & \text{under}\quad\mathcal{H}_0\\ \mathcal{N}\left(\delta_Q(\boldsymbol{x}_T,\boldsymbol{\gamma}),1\right) & \text{under}\quad\mathcal{H}_1\end{cases},\tag{25}$$

The non-centrality $\lambda_Q(\boldsymbol{x}_T,\boldsymbol{\tau})\triangleq(\theta_1-\theta_0)^2\,\mathrm{I}(\theta_0,\boldsymbol{x}_T)$ and the deflection $\delta_Q(\boldsymbol{x}_T,\boldsymbol{\gamma})\triangleq(P_{\theta_1}-P_{\theta_0})\,\sqrt{\mathrm{I}(P_{\theta_0},\boldsymbol{x}_T,\boldsymbol{\gamma})}$ measures[6] in Eqs. (24) and (25), respectively, are given as:

$$\lambda_Q(\boldsymbol{x}_T,\boldsymbol{\tau})=\theta_1^2\sum_{k=1}^{K}\psi_{0,k}^{\rm rq}(\tau_k)\,g^2(\boldsymbol{x}_T,\boldsymbol{x}_k)\,;\tag{26}$$

$$\delta_Q(\boldsymbol{x}_T,\boldsymbol{\gamma})=P_{\theta_1}\sqrt{\sum_{k=1}^{K}\psi_{0,k}^{\rm sq}(\gamma_k)\,g^4(\boldsymbol{x}_T,\boldsymbol{x}_k)}\,.\tag{27}$$

Additionally, they are reported as a function of $(\boldsymbol{x}_T,\boldsymbol{\tau})$ and $(\boldsymbol{x}_T,\boldsymbol{\gamma})$, respectively, to stress the dependence on the unknown position $\boldsymbol{x}_T$ and the vector of variables to optimize ($\boldsymbol{\tau}$ or $\boldsymbol{\gamma}$). Finally, the terms θ_1 and P_{θ_1} represent the *true values of the target signal* and *power,* respectively, under $\mathcal{H}_1$.

Clearly the larger $\lambda_Q(\boldsymbol{x}_T,\boldsymbol{\tau})$ and $\delta_Q(\boldsymbol{x}_T,\boldsymbol{\gamma})$ are, the better the $\boldsymbol{x}_T-$clairvoyant Rao and LOD tests, respectively, will perform when the target to be detected is located at $\boldsymbol{x}_T$. The

[5]That is $|\theta_1-\theta_0|=c/\sqrt{K}$ for a certain value $c>0$ [20].

[6]We employ the slightly-modified notations $\mathrm{I}(\theta,\boldsymbol{x}_T,\boldsymbol{\tau})$ and $\psi_{0,k}^{\rm rq}(\tau_k)$ (resp. $\mathrm{I}(P_\theta,\boldsymbol{x}_T,\boldsymbol{\gamma})$ and $\psi_{0,k}^{\rm sq}(\gamma_k)$), as opposed to $\mathrm{I}(\theta,\boldsymbol{x}_T)$ and $\psi_{0,k}^{\rm rq}$ (resp. $\mathrm{I}(P_\theta,\boldsymbol{x}_T)$ and $\psi_{0,k}^{\rm sq}$), to stress the dependence on thresholds τ_k's. (resp. γ_k's).

same applies to the $\boldsymbol{x}_T-$clairvoyant GLR on either quantizer-originated data. For this reason, we aim to design the threshold vectors $\boldsymbol{\tau}$ and $\boldsymbol{\gamma}$, respectively, as

$$\boldsymbol{\tau}^\star \triangleq \arg\max_{\boldsymbol{\tau}} \ \lambda_Q(\boldsymbol{x}_T, \boldsymbol{\tau})\,; \tag{28}$$

$$\boldsymbol{\gamma}^\star \triangleq \arg\max_{\boldsymbol{\gamma}} \ \delta_Q(\boldsymbol{x}_T, \boldsymbol{\gamma})\,. \tag{29}$$

However, by doing so, we could potentially obtain (impractical) solutions $\boldsymbol{\tau}^\star$ and $\boldsymbol{\gamma}^\star$ which depend on $\boldsymbol{x}_T$. Luckily, for this particular problem, the optimization simplifies into K *decoupled* threshold designs (hence the optimization complexity scales linearly with the number of sensors K), whose solutions are also independent of $\boldsymbol{x}_T$ (cf. Eqs. (26) and (27)).

Indeed, for the G-Rao case, it holds (for each k):

$$\max_{\tau_k} \left\{ \psi_{0,k}^{\mathrm{rq}}(\tau_k) = \frac{\mu_{h,k}^2}{\sigma_{w,k}^2} \frac{p_{\mathcal{N}}^2\left(\tau_k \,/\, \sqrt{\sigma_{w,k}^2}\right)}{\Delta_k + \beta_{0,k}(\tau_k)\left[1-\beta_{0,k}(\tau_k)\right]} \right\} \tag{30}$$

where $\Delta_k \triangleq [P_{e,k}\,(1-P_{e,k})]/(1-2P_{e,k})^2$. The aforementioned objective is shown in Fig. 2a for different values of $P_{e,k}$, and κ. It is known from the quantized estimation literature [32], [33] that for Gaussian pdf $\tau_k^\star \triangleq \arg\max_{\tau_k} \psi_{0,k}^{\mathrm{rq}}(\tau_k) = 0$ when $\Delta_k = 0$ (corresponding to $P_{e,k} = 0$). However, it is not difficult to show[7] that this result holds for any value of $\Delta_k \neq 0$, which corresponds to different conditions of the noisy ($P_{e,k} \neq 0$) reporting channels. It is worth noticing that the objective maximizer in Eq. (30) coincides with the one obtained for the case of a purely-deterministic (LoS) parameter in [15] and is thus *independent* of the specific LoS/NLoS relative weight.

Differently, for the G-LOD case, we have (for each k):

$$\max_{\gamma_k} \left\{ \psi_{0,k}^{\mathrm{sq}}(\gamma_k) = \frac{(\mu_{h,k}^2 + \sigma_{h,k}^2)^2}{(\sigma_{w,k}^2)^2} \times \frac{p_{\mathcal{N}}^2\left(\sqrt{\gamma_k/\sigma_{w,k}^2}\right)(\gamma_k/\sigma_{w,k}^2)}{\Delta_k + \rho_{0,k}(\gamma_k)\left[1-\rho_{0,k}(\gamma_k)\right]} \right\} \tag{31}$$

Such maximization can be re-formulated in terms of the sensor false-alarm probability $\rho_{0,k}$ (being in *bijective* correspondence with γ_k), as

$$\psi_{0,k}^{\mathrm{sq}}(\rho_{0,k}) = \frac{(\mu_{h,k}^2 + \sigma_{h,k}^2)^2}{(\sigma_{w,k}^2)^2} \times \frac{p_{\mathcal{N}}^2(\mathcal{Q}^{-1}(\rho_{0,k}/2))\,\left[\mathcal{Q}^{-1}(\rho_{0,k}/2)\right]^2}{\Delta_k + \rho_{0,k}\,(1-\rho_{0,k})} \tag{32}$$

The aforementioned objective is shown in Fig. 2b for different values of $P_{e,k}$ and κ. The optimized $\rho_{0,k}^\star$ can be easily evaluated via a 1-D line search. It is worth noticing that the objective maximizer in Eq. (32) coincides with the one obtained for the case of a purely-random (NLoS) parameter in [23] and is thus independent on the specific LoS/NLoS relative weight.

Remarks: although optimization of both raw- and square-quantizer thresholds has been to shown to be independent of the specific LoS/NLoS relative weight, we stress that detection performance in both cases is going to depend significantly on the above parameter instead. Indeed, we observe that the (optimized) non-centrality $\lambda_Q(\boldsymbol{x}_T, \boldsymbol{\tau})$ grows, via the terms $\psi_{0,k}^{\mathrm{rq}}(\tau_k)$, $k = 1, \dots K$, with $\mu_{h,k}^2 \,/\, \sigma_{w,k}^2$ (see Eq. (30)). Conversely, the (optimized) non-centrality $\delta_Q(\boldsymbol{x}_T, \boldsymbol{\gamma})$ grows, via the terms $\psi_{0,k}^{\mathrm{sq}}(\rho_{0,k})$, $k = 1, \dots K$, with $(\mu_{h,k}^2 + \sigma_{h,k}^2) \,/\, \sigma_{w,k}^2$ (see Eq. (32)). Hence, the above observations highlight that: (a) the performance of G-LOD is likely to be weakly-dependent over a wide range of LoS/NLoS relative conditions (because of the presence of the sum $\mu_{h,k}^2 + \sigma_{h,k}^2$), (b) G-Rao is expected to suffer from severe performance degradation when NLoS terms become dominant (because of the absence of $\sigma_{h,k}^2$) and (c) in highly-LoS conditions we expect a more sensible gain achieved by G-Rao at low SNR as the result of the squaring of $(\mu_{h,k}^2 + \sigma_{h,k}^2) \,/\, \sigma_{w,k}^2$ in Eq. (32).

V. Numerical Results and Discussion

Simulation setup: Herein, we compare the numerical performance of the optimized G-Rao, G-LOD and GLR tests, based on the threshold-optimization design proposed in Sec. IV. Specifically, our simulation setup considers a 2-D ($\boldsymbol{x}_T \in \mathbb{R}^2$) square area defined as $\mathcal{A} \triangleq [0,1]^2$, in which a non-cooperative target is detected by a WSN with $K = 49$ sensors. For simplicity, the nodes are arranged to uniformly cover the whole $\mathcal{A}$ in a grid fashion. Regarding the sensing model, the AAF considered is a power-law, namely

$$g(\boldsymbol{x}_T, \boldsymbol{x}_k) \triangleq 1 \,/\, \sqrt{1 + (\|\boldsymbol{x}_T - \boldsymbol{x}_k\| \,/\, \eta)^\alpha} \tag{33}$$

where we have set $\eta = 0.2$ (viz. approximate target extent) and $\alpha = 4$ (viz. decay exponent). Also, for simplicity, $w_k \sim \mathcal{N}(0, \sigma_w^2 = 1)$ and $\mu_h^2 = 1$, $k \in \mathcal{K}$. Initially, we assume error-free BSCs, namely $P_{e,k} = 0$, $k \in \mathcal{K}$. All the simulations are based on 10^5 Monte Carlo runs.

Based on Sec. III, the implementation of Λ_{GLR}, Λ_{GRao} and Λ_{GLOD} leverages grid search. Specifically, the search space of the target signal θ (resp. power P_θ) is assumed to be $S_\theta \triangleq \left[-\bar{\theta}, \bar{\theta}\right]$ (resp. $S_{P_\theta} \triangleq [0, P_{\bar{\theta}}]$), where $\bar{\theta} > 0$ (resp. $P_{\bar{\theta}} > 0$) is such that the $\mathrm{SNR} = 20\,\mathrm{dB}$. The vector collecting the points on the grid is then defined as $\left[-\boldsymbol{g}_\theta^T \quad 0 \quad \boldsymbol{g}_\theta^T\right]^T$ (resp. $\left[0 \quad \boldsymbol{g}_{P_\theta}^T\right]$), where $\boldsymbol{g}_\theta$ (resp. $\boldsymbol{g}_{P_\theta}$) collects target strengths

[7] Indeed, the inequality $p_{\mathcal{N}}^2\left(\tau_k^\circ\right) \,/\, \left\{\Delta_k + \mathcal{Q}(\tau_k^\circ)\left[1-\mathcal{Q}(\tau_k^\circ)\right]\right\} \leq p_{\mathcal{N}}^2(0) \,/\, \{\Delta_k + \mathcal{Q}(0)\,[1-\mathcal{Q}(0)]\}$, where $\tau_k^\circ \triangleq \tau_k \,/\, \sqrt{\sigma_{w,k}^2}$, can be rewritten as

$$\left\{p_{\mathcal{N}}^2\left(\tau_k^\circ\right)\mathcal{Q}(0)\left[1-\mathcal{Q}(0)\right] - p_{\mathcal{N}}^2(0)\,\mathcal{Q}(\tau_k^\circ)\left[1-\mathcal{Q}(\tau_k^\circ)\right]\right\} + \Delta_k\left\{p_{\mathcal{N}}^2\left(\tau_k^\circ\right) - p_{\mathcal{N}}^2(0)\right\} \leq 0$$

The above condition is always satisfied since the negativity of first term within the curly brackets follows directly from the result for ideal BSCs ($\Delta_k = 0$) [32], [34], while for the second term both (a) $\Delta_k > 0$ and (b) $\left\{p_{\mathcal{N}}^2\left(\tau_k^\circ\right) - p_{\mathcal{N}}^2(0)\right\} \leq 0$ (because the normal distribution attains its mode at zero) hold.

(power values) corresponding to the SNR values $-10 : 2.5 : 20\,(\mathrm{dB})$. As a result, the number of amplitude and power bins equals $N_\theta = 25$ and $N_{P_\theta} = 13$, respectively. Secondly, the search support of $\boldsymbol{x}_T$ coincides with the monitored area ($\mathrm{S}_{\boldsymbol{x}_T} = \mathcal{A}$). Accordingly, the 2-D grid is the result of sampling $\mathcal{A}$ uniformly with $N_{\boldsymbol{x}_T} = N_c^2$ points, where $N_c = 100$. In this setup, the evaluation of G-Rao (G-LOD) requires $N_c^2 = 10^4$ grid points, as opposed to $N_c^2 N_\theta = 2.5 \times 10^5$ (resp. $N_c^2 N_{P_\theta} = 1.3 \times 10^5$) points for GLR. This leads to a > 20 *(resp.* > 10 *) times* lower complexity of G-Rao (G-LOD) with respect to a GLR based on the same quantization strategy.

Considered Baselines: For the sake of a complete comparison and to assess the loss due to quantization, we consider the following baselines: (i) a GLR having available the full-precision measurements z_k's, (ii) G-Rao and (iii) G-LOD tests based on the same data. Regarding (i), its (implicit) expression is analogous to that in Eq. (8) and is implemented via the following explicit expression:

$$\Lambda_{\mathrm{GLR}}^{\mathrm{fp}}(\boldsymbol{z}) = \max_{(\boldsymbol{x}_T,\theta)} \sum_{k=1}^{K} \left\{ \log\left[\sigma_{w,k}^2 \,/\, \sigma_{\mathrm{eq},k}^2(\theta)\right] \right.$$
$$\left. \left[z_k^2 \,/\, \sigma_{\mathrm{eq},k}^2(\theta)\right] - \left[(z_k - g_k\,\mu_{h,k}\,\theta)^2 \,/\, \sigma_{\mathrm{eq},k}^2(\theta)\right] \right\} \tag{34}$$

For (ii) and (iii), their explicit expressions (the proof is not included for brevity) are respectively given as

$$\Lambda_{\mathrm{GRao}}^{\mathrm{fp}}(\boldsymbol{z}) \triangleq \max_{\boldsymbol{x}_T} \frac{\left(\sum_{k=1}^{K} g_k\,\mu_{h,k}\,z_k/\sigma_{w,k}^2\right)^2}{\sum_{k=1}^{K} g_k^2\,\mu_{h,k}^2\,/\,\sigma_{w,k}^2} \tag{35}$$

$$\Lambda_{\mathrm{GLOD}}^{\mathrm{fp}}(\boldsymbol{z}) \triangleq \max_{\boldsymbol{x}_T} \frac{\sum_{k=1}^{K} \frac{1}{2}\left[\frac{g_k^2}{\sigma_{w,k}^2}(\mu_{h,k}^2 + \sigma_{h,k}^2)\left(\frac{z_k^2}{\sigma_{w,k}^2} - 1\right)\right]}{\sqrt{\frac{1}{2}\sum_{k=1}^{K} \frac{g_k^4}{\sigma_{w,k}^4}(\mu_{h,k}^2 + \sigma_{h,k}^2)^2}} \tag{36}$$

We remark that, in order to apply G-LOD, the derivation is actually performed starting from the square values z_k^2 (leading to an analogous change of the nature of the test from two-sided to one-sided as in the one-bit quantization case).

Discussion of Results: First, Fig. 3 provides a P_{D} comparison (subject to $P_F = 0.01$) of considered fusion rules versus κ (dB), to assess their detection sensitivity versus the LoS/NLoS relative terms ratio emitted by the non-cooperative target. In the present analysis, the target position $\boldsymbol{x}_T$ is randomly sampled within $\mathcal{A}$ at each run (when $\mathcal{H}_1$ is drawn). We consider a sensing $\mathrm{SNR} = 10\,\mathrm{dB}$ for the target. Results highlight that G-LOD$^{\mathrm{sq}}$ performs as well as a GLR$^{\mathrm{sq}}$ and outperforms both G-Rao and GLR based on RQ, over the whole κ range. The observation of the performance for tests based on full-precision highlight (i) the loss due to quantization and (ii) problems related to considering a Rao test for the multiplicative fading case, especially in a low κ condition.

Then, in Fig. 4 we perform a P_{D} comparison (subject to $P_F = 0.01$) of considered fusion rules versus SNR (dB), to assess their detection rate versus the sensing SNR for two different conditions of "scatteredness", namely $\kappa = 0\,\mathrm{dB}$ and $\kappa = 10\,\mathrm{dB}$. Results highlight the close match between the GLR and the corresponding generalized score test (G-Rao or G-LOD) based on the same type of data (i.e. FP, RQ or SQ). By comparing G-Rao$^{\mathrm{rq}}$ and G-LOD$^{\mathrm{sq}}$, it is apparent that their relative performance depends on the scatteredness condition. For example, while for high-LoS, G-Rao$^{\mathrm{rq}}$ performs better, in the case of low-LoS, the advantage of G-LOD$^{\mathrm{sq}}$ becomes apparent. The advantage of the squaring operation is also evident from the performance gap reduction achieved by G-LOD$^{\mathrm{fp}}$ with respect to GLR$^{\mathrm{sq}}$ and G-Rao$^{\mathrm{fp}}$.

As a complementary analysis, in Fig. 5 we deepen the P_{D} comparison (subject to $P_F = 0.01$) by analyzing a variable number of sensors K. In detail, we consider the same square surveillance area $\mathcal{A} = [0, 1]^2$, but we assume a linear increase of the number of sensors on the grid length (i.e. a

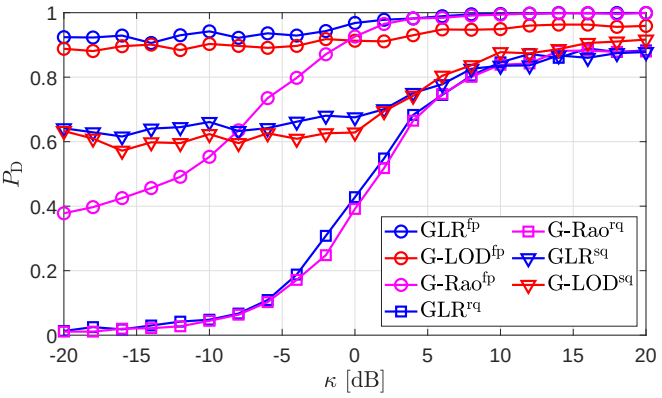

Figure 3: P_{D} vs. κ factor (dB); false-alarm probability at FC is set to $P_{\mathrm{F}} = 0.01$. A WSN with $K = 49$ sensors and a target with $\mathrm{SNR} = 10\,\mathrm{dB}$ is considered. The sensor thresholds for RQ and SQ are set according to the design reported in Sec. IV.

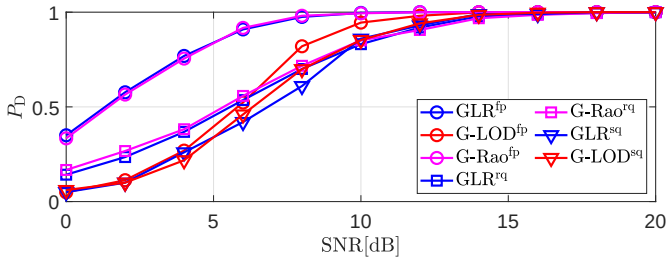

(a) $\kappa = 10\,\mathrm{dB}$;

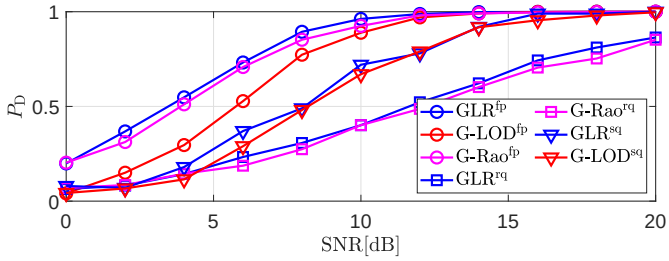

(b) $\kappa = 0\,\mathrm{dB}$;

Figure 4: P_{D} vs. SNR (dB); false-alarm probability at FC is set to $P_{\mathrm{F}} = 0.01$. A WSN with $K = 49$ sensors is considered. Sensor thresholds for RQ and SQ-based rules are set according to Sec. IV.

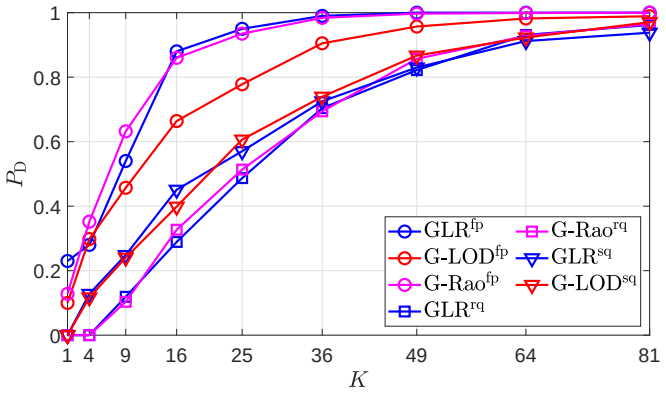

Figure 5: P_D vs. number of sensors K; false-alarm probability at FC is set to $P_F = 0.01$. A target with SNR $= 10\,$dB and $\kappa = 10\,$dB is considered. Sensor thresholds for RQ and SQ-based rules are set according to Sec. IV.

quadratic grow of K) so as to investigate the effect of WSN grid densification on the system detection rate. As expected, all the considered fusion rules benefit from a finer grid of sensors monitoring the target to be detected, with the rules based on FP achieving near-ideal performance with a lower number of sensors (i.e. a coarser grid). Differently, concerning fusion rules based on one-bit quantization, those based on SQ achieve slightly improved performance for lower values of K. Differently, as the WSN densification grows, such gain over RQ-based rules reduces. For instance, when targeting $P_D \approx 0.8$ (resp. $P_D \approx 0.9$) a uniform grid with $K = 49$ (resp. $K = 64$) sensors suffices for both RQ-based and SQ-basd rules.

A more in depth comparison of G-LOD^{sq} and G-Rao^{rq} along the κ and SNR dimensions is reported in Fig. 6. Specifically, we present the P_D vs. (κ, SNR) (dB) for a FC false-alarm probability set to $P_F = 0.01$ for G-LOD^{sq} (left) and G-Rao^{rq} (center), respectively, and their difference ΔP_D (right). From the inspection of results, we can infer how G-Rao^{rq} is highly sensitive to low values of κ (NLoS condition). Differently, G-LOD^{sq} is almost insensitive to the specific Los/NLoS condition (viz. the value of κ). The performances of both fusion rules degrade with a decreasing SNR. By comparing the performance of both rules (via the difference $\Delta P_D \triangleq (P_D^{GLOD} - P_D^{GRao})$) over the whole (κ, SNR) plane, it is apparent how high SNR and high κ represents the region where G-LOD^{sq} "wins", whereas an opposite outcome is observed in the case of low SNR and low κ (i.e. G-Rao^{rq} wins). Still, in the latter case, the performance gain ensured by G-Rao^{rq} over G-LOD^{sq} (right figure) is not as high as the winning G-LOD^{sq} region. Such results may be explained by looking at the terms $\psi_{0,k}^{rq}(\tau_k)$ and $\psi_{0,k}^{sq}(\rho_{0,k})$ (cf. Eqs. (30) and (32), respectively), and their relative trends highlighted at the end of Sec. IV. Indeed, $\psi_{0,k}^{rq}(\tau_k)$ and $\psi_{0,k}^{sq}(\rho_{0,k})$ directly influence the value of the $\boldsymbol{x}_T$-clairvoyant non-centrality parameters $\lambda_Q(\boldsymbol{x}_T, \boldsymbol{\tau})$ and $\delta_Q(\boldsymbol{x}_T, \boldsymbol{\gamma})$, respectively, which limit (from the above) the achievable performance of G-Rao^{rq} and G-LOD^{sq}.

We then delve into the analysis of the effect of the reporting errors by means of Fig. 7. The latter provides a P_D comparison (subject to $P_F = 0.01$) of the seven fusion rules versus $P_{e,k} = P_e$, $k \in \mathcal{K}$ (i.e. the same BEP for all the sensors). Two different scatteredness cases are considered, namely $\kappa = 0\,$dB (Fig. 7a) and $\kappa = 5\,$dB (Fig. 7b). Results highlight that BEP (viz. P_e) increase has a detrimental effect on *all* the RQ/SQ-based rules and further enlarges their gap with respect to FP-based counterparts. Remarkably, in the case of $\kappa = 5\,$dB, the benefits of SQ (over RQ) are almost nullified when $P_e \approx 0.15$.

Finally, we investigate the detection coverage properties of the considered fusion rules over the entire surveillance area $\mathcal{A}$. To this end, in Fig. 8, we report P_D (under $P_F = 0.01$) versus the target location $\boldsymbol{x}_T$ (for SNR $= 5\,$dB and $\kappa = 0\,$dB) for all the rules considered, except of G-Rao^{fp}, due to its poor performance in this peculiar NLoS configuration. It is apparent that the $P_D(\boldsymbol{x}_T)$ surface is similar for all the rules from a qualitative viewpoint. Also, it underlines lower detection performance at the edges of the surveillance area. This outcome arises from the regular WSN placement within $\mathcal{A}$ for the scenario analyzed. From the comparison among the different rules, it is apparent that the G-LOD^{sq} test presents only marginal loss with respect to the GLR^{sq}, and significant gain with respect to G-Rao^{rq} and GLR^{rq}. Clearly, the detection coverage is not as good as the FP counterparts considered, due to the degrading effect of parsimonious (one-bit) quantization.

VI. Conclusions and Future Directions

In this work, we devised a WSN-based DD scheme in the presence of (a) multiplicative fading, (b) quantized measurements, (c) non-ideal and non-identical BSCs. The target to be detected emits an unknown (since it is non-cooperative) deterministic signal (θ) from unknown location ($\boldsymbol{x}_T$), Since $\boldsymbol{x}_T$ is a nuisance parameter present only under $\mathcal{H}_1$ (i.e. when $\theta \neq 0$), we designed generalized versions of the Rao and LOD tests as attractive (low-complexity) alternatives to GLR (the latter requiring a grid search on the whole space $(\theta, \boldsymbol{x}_T)$) based on the same quantization choice. These generalized forms were obtained from the framework in [28]. The resulting forms of G-Rao and G-LOD require single maximization (with respect to $\boldsymbol{x}_T$) of a family of $\boldsymbol{x}_T$-conditional decision statistics, obtained by assuming $\boldsymbol{x}_T$ known, thus avoiding the need for grid search over θ (or P_θ). Further, we developed an effective criterion (drawn from semi-theoretical performance) to optimize sensor thresholds of either quantization type (RQ or SQ). This resulted in a zero-threshold choice for RQ and a simple 1-D search for SQ. Also, these outcomes were shown to be independent of the specific κ value. Numerical results for G-LOD^{sq} underlined (i) similar P_D values to both G-Rao^{rq} and GLR^{rq} in the LoS case, (ii) similar performance of GLR^{sq} in the NLoS case, (iii) high gains with respect to G-Rao^{rq} over a relevant κ range. Accordingly, we believe the adoption of SQ with G-LOD^{sq} represents an appealing design choice for DD in such scenario for a wide range of Los/NLoS conditions. The sole exception is represented by highly-LOS low-SNR

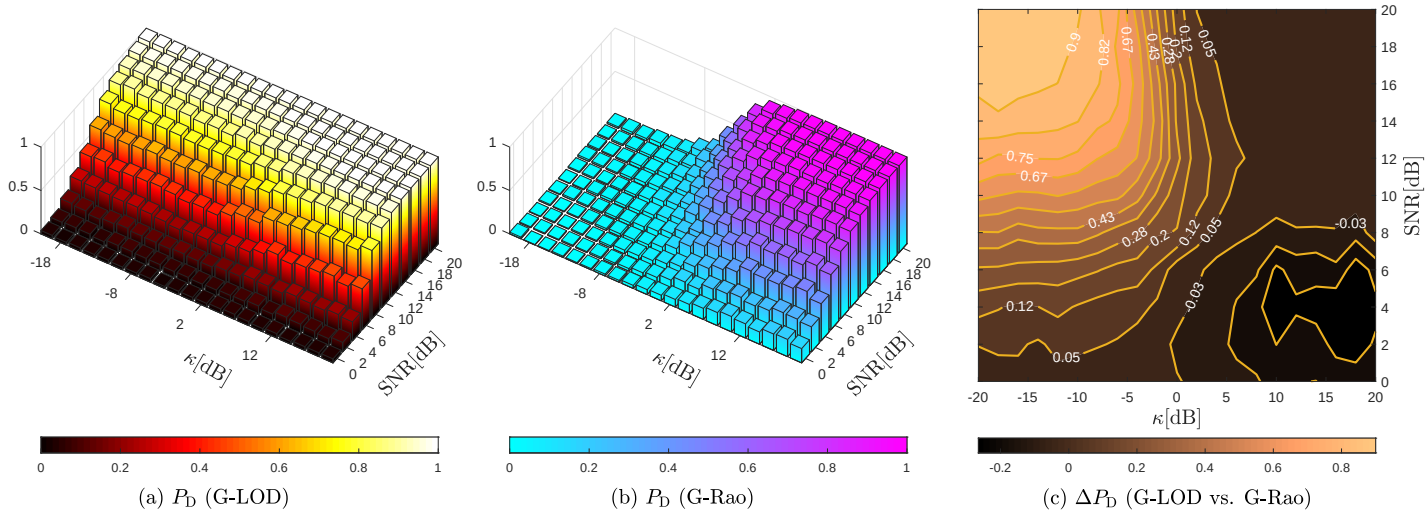

(a) $P_{\rm D}$ (G-LOD) (b) $P_{\rm D}$ (G-Rao) (c) $\Delta P_{\rm D}$ (G-LOD vs. G-Rao)

Figure 6: Comparison of G-LOD$^{\rm sq}$ and G-Rao$^{\rm rq}$ for a randomly-generated target. $P_{\rm D}$ vs. (κ, SNR) (dB) for a FC false-alarm probability set to $P_{\rm F} = 0.01$ for G-LOD$^{\rm sq}$ (a) and G-Rao$^{\rm rq}$ (b), respectively, and (c) their difference $\Delta P_{\rm D} \triangleq (P_{\rm D}^{\rm GLOD} - P_{\rm D}^{\rm GRao})$. A WSN with $K = 49$ sensors is considered: their thresholds are optimized as in Sec. IV; ideal BSCs are assumed, i.e. $P_{e,k} = 0$.

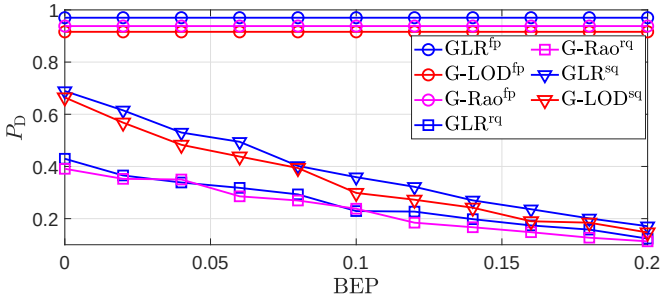

(a) $\kappa \in 0\,$dB;

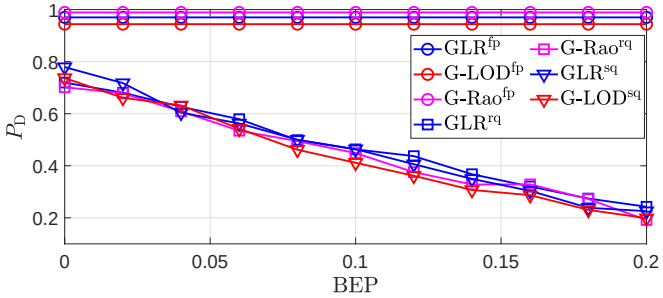

(b) $\kappa \in 5\,$dB;

Figure 7: $P_{\rm D}$ vs. BEP ($P_{e,k} = P_e$); the FC false-alarm probability is set to $P_{\rm F} = 0.01$. A WSN with $K = 49$ sensors and a target with sensing SNR $= 10\,$dB are considered.

scenarios, where the joint use of RQ and G-Rao test at the FC should be preferred.

Future directions of research will investigate DD via sensor fusion in more challenging and close-to-real contexts. These include multi-bit quantizers [35], robustness to phy-layer attacks [36], time-correlated reporting channels [37], multidimensional measurement models [38], incompletely-specified noise and model pdfs (e.g. unknown AAF), models enjoying sparsity [8] and energy-efficient censoring sensors. Additionally, the derivation of (asymptotic) theoretical expressions for the detection ($P_{\rm D}$) and false-alarm ($P_{\rm F}$) probabilities of generalized score tests is also foreseen as a (challenging) avenue for future research.

Appendix A
Derivation of the Score Functions

In this Appendix, we derive the $\boldsymbol{x}_T$-conditional score functions for G-Rao and G-LOD tests, namely $\partial \log[P(\hat{\boldsymbol{b}}; \theta, \boldsymbol{x}_T)/\partial\theta]$ and (i.e. $\partial \log[P(\hat{\boldsymbol{d}}; P_\theta, \boldsymbol{x}_T)/\partial P_\theta]$, evaluated at θ_0 and P_{θ_0}, respectively.

We first focus on the score function needed for G-Rao evaluation. Precisely, based on the factorization form in Eq. (7), the log-likelihood function $\log P(\hat{\boldsymbol{b}}; \theta, \boldsymbol{x}_T)$ is given by

$$\log P(\hat{\boldsymbol{b}}; \theta, \boldsymbol{x}_T) \tag{37}$$
$$= \sum_{k=1}^{K} \{\widehat{b}_k \, \log[\alpha_k^{\rm rq}(\theta, \boldsymbol{x}_T)] + (1 - \widehat{b}_k) \, \log[1 - \alpha_k^{\rm rq}(\theta, \boldsymbol{x}_T)]\}$$

Taking the derivative of $\log P(\hat{\boldsymbol{b}}; \theta, \boldsymbol{x}_T)$ with respect to θ, we write the corresponding expression as (due to independence)

$$\frac{\partial \log P(\hat{\boldsymbol{b}}; \theta, \boldsymbol{x}_T)}{\partial \theta} = \sum_{k=1}^{K} \frac{P'(\hat{b}_k; \theta, \boldsymbol{x}_T)}{P(\hat{b}_k; \theta, \boldsymbol{x}_T)} \tag{38}$$
$$= \sum_{k=1}^{K} \frac{\partial \alpha_k^{\rm rq}(\theta, \boldsymbol{x}_T)}{\partial \theta} \, \frac{\left(\hat{b}_k - \alpha_k^{\rm rq}(\theta, \boldsymbol{x}_T)\right)}{\alpha_k^{\rm rq}(\theta, \boldsymbol{x}_T)\,[1 - \alpha_k^{\rm rq}(\theta, \boldsymbol{x}_T)]},$$

According to the bit probability model in Eq. (4), the derivative of the $\alpha_k^{\rm rq}(\theta, \boldsymbol{x}_T)$ with respect to θ is given explicitly as:

$$\frac{\partial \alpha_k^{\rm rq}(\theta, \boldsymbol{x}_T)}{\partial \theta} = (1 - 2P_{e,k})\, p_{\mathcal{N}} \left(\frac{\tau_k - g_k\, \mu_{h,k}\, \theta}{\sqrt{\sigma_{{\rm eq},k}^2(\theta)}} \right) \times \frac{\left(\tau_k\, g_k^2\, \sigma_{h,k}^2 \theta + g_k\, \mu_{h,k}\, \sigma_{w,k}^2\right)}{[\sigma_{{\rm eq},k}(\theta)]^{3/2}} \tag{39}$$

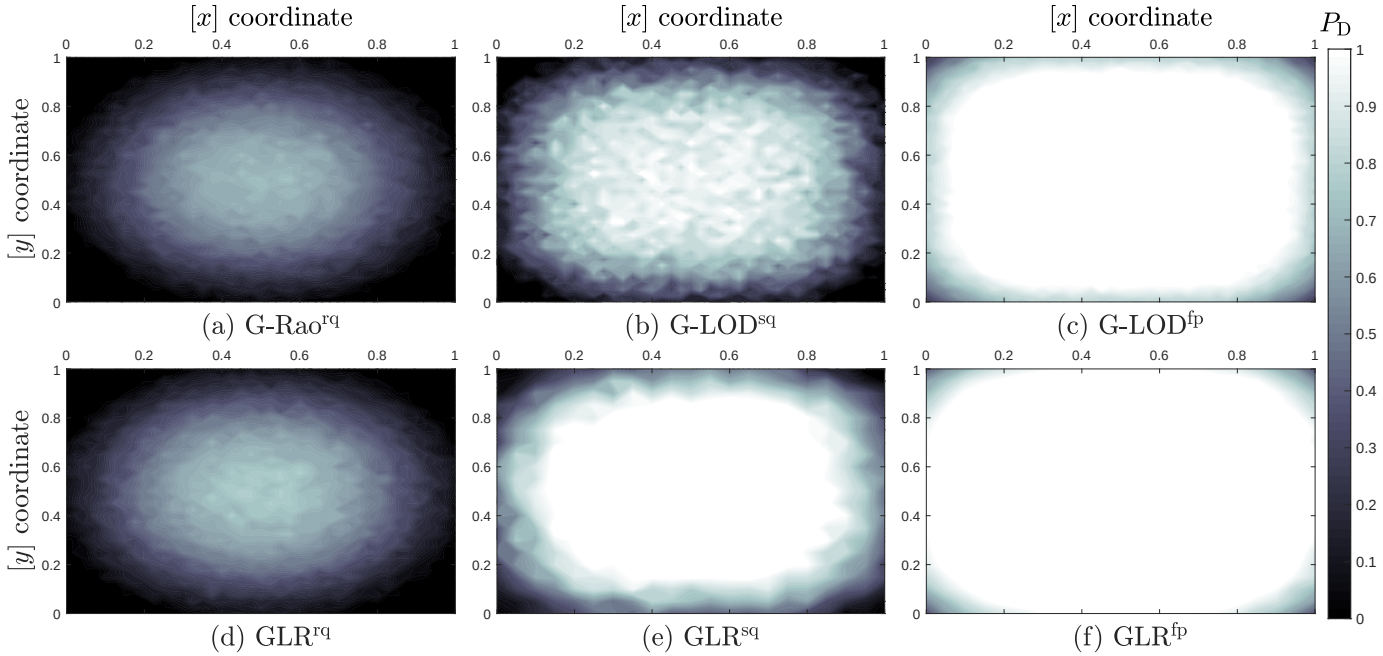

Figure 8: $P_{\rm D}$ heatmaps vs. target position $\boldsymbol{x}_T$ for (a) G-Rao$^{\rm rq}$, (b) G-LOD$^{\rm sq}$, (d) GLR$^{\rm rq}$ and (e) GLR$^{\rm sq}$. For completeness, also the best two full-precision baselines ((c) and (f), corresponding to GLR$^{\rm fp}$ and G-LOD$^{\rm fp}$, respectively) are reported. The FC false-alarm probability is set to $P_{\rm F} = 0.01$. A WSN with $K = 49$ sensors and a target with sensing $\mathrm{SNR} = 5\,\mathrm{dB}$ and $\kappa = 0\,\mathrm{dB}$ are considered. Corresponding decisions are sent over BSCs with $P_{{\rm e},k} = 0.1$. The sensor thresholds for RQ and SQ are set according to the design reported in Sec. IV.

Evaluating the derivative of the log-pdf in Eq. (38) at $\theta = \theta_0$ (corresponding to the null hypothesis $\mathcal{H}_0$), leads to:

$$\left.\frac{\partial \log P(\hat{\boldsymbol{b}};\theta,\boldsymbol{x}_T)}{\partial\theta}\right|_{\theta=\theta_0} = \sum_{k=1}^{K} \left.\frac{\partial \alpha_k^{\rm rq}(\theta,\boldsymbol{x}_T)}{\partial\theta}\right|_{\theta=\theta_0} \frac{\left(\hat{b}_k - \alpha_{0,k}^{\rm rq}\right)}{\alpha_{0,k}^{\rm rq}\left[1-\alpha_{0,k}^{\rm rq}\right]} \tag{40}$$

and, in turn

$$\left.\frac{\partial \alpha_k^{\rm rq}(\theta,\boldsymbol{x}_T)}{\partial\theta}\right|_{\theta=\theta_0} = (1-2P_{e,k})\, p_{\mathcal{N}}\left(\frac{\tau_k}{\sqrt{\sigma_{w,k}^2}}\right)\frac{g_k\,\mu_{h,k}}{\sigma_{w,k}} \tag{41}$$

Then, exploiting the appropriate substitutions, we obtain:

$$\left.\frac{\partial \log P(\hat{\boldsymbol{b}};\theta,\boldsymbol{x}_T)}{\partial\theta}\right|_{\theta=\theta_0} = \sum_{k=1}^{K}\left\{\frac{\left(\hat{b}_k - \alpha_{0,k}^{\rm rq}\right)}{\alpha_{0,k}^{\rm rq}\left[1-\alpha_{0,k}^{\rm rq}\right]} \times (1-2P_{e,k})\, p_{\mathcal{N}}\left(\frac{\tau_k}{\sqrt{\sigma_{w,k}^2}}\right)\frac{g_k\,\mu_{h,k}}{\sigma_{w,k}}\right\} \tag{42}$$

By defining the auxiliary quantity

$$\Xi_k^{\rm rq} \triangleq \frac{(1-2P_{{\rm e},k})}{\alpha_{0,k}^{\rm rq}\left[1-\alpha_{0,k}^{\rm rq}\right]}\,\frac{\mu_{h,k}}{\sigma_{w,k}}\,p_{\mathcal{N}}\left(\tau_k \,/\, \sqrt{\sigma_{w,k}^2}\right) \tag{43}$$

we obtain the final expression

$$\left.\frac{\partial \log P(\hat{\boldsymbol{b}};\theta,\boldsymbol{x}_T)}{\partial\theta}\right|_{\theta=\theta_0} = \sum_{k=1}^{K}\left(\hat{b}_k - \alpha_{0,k}^{\rm rq}\right)\Xi_k^{\rm rq}\, g_k \tag{44}$$

Differently, referring to the $\boldsymbol{x}_T$-conditional score function needed for G-LOD evaluation, we observe that $\log P(\hat{\boldsymbol{d}};P_\theta,\boldsymbol{x}_T)$ admits a similar additive form as Eq. (37). Accordingly, $\partial \log P(\hat{\boldsymbol{d}};P_\theta,\boldsymbol{x}_T)\,/\,\partial P_\theta$ can be rewritten similarly as the last line of Eq. (38) if we replace $\hat{b}_k$, $\alpha_k^{\rm rq}(\theta,\boldsymbol{x}_T)$ and $\partial\alpha_k^{\rm rq}(\theta,\boldsymbol{x}_T)/\partial\theta$ with $\hat{d}_k$, $\alpha_k^{\rm sq}(P_\theta,\boldsymbol{x}_T)$ and $\partial\alpha_k^{\rm sq}(P_\theta,\boldsymbol{x}_T)\,/\,\partial P_\theta$, respectively.

Based on the bit probability model in Eq. (6), the derivative of $\alpha_k^{\rm sq}(P_\theta,\boldsymbol{x}_T)$ with respect to P_θ is more involved and given explicitly as in Eq. (45), at the top of next page.

Evaluating the derivative of the log-pdf in (38) at $P_\theta = P_{\theta_0}$ (corresponding to the null hypothesis $\mathcal{H}_0$), leads to:

$$\left.\frac{\partial \log P(\hat{\boldsymbol{d}};P_\theta,\boldsymbol{x}_T)}{\partial P_\theta}\right|_{P_\theta=P_{\theta_0}} = \sum_{k=1}^{K}\left(\lim_{P_\theta\to P_{\theta_0}}\frac{\partial\alpha_k^{\rm sq}(P_\theta,\boldsymbol{x}_T)}{\partial P\theta}\right)\frac{\left(\hat{d}_k - \alpha_{0,k}^{\rm sq}\right)}{\alpha_{0,k}^{\rm sq}\left[1-\alpha_{0,k}^{\rm sq}\right]} \tag{46}$$

The above limit is an undetermined form of the type $\frac{0}{0}$ and its explicit solution (obtained by leveraging $\lim_{x\to 0}[\exp(x) -$

$$\frac{\partial \alpha_k^{\rm sq}(P_\theta,\boldsymbol{x}_T)}{\partial P_\theta} = (1-2P_{e,k}) \times \left\{ \frac{|g_k|\,|\mu_{h,k}|\,\sigma_{w,k}^2}{2\sqrt{P_\theta}\left[\sigma_{{\rm eq},k}(P_\theta)\right]^3} \left[-p_{\mathcal{N}}\left(\frac{\sqrt{\gamma_k}+|g_k|\,|\mu_{h,k}|\,\sqrt{P_\theta}}{\sqrt{\sigma_{{\rm eq},k}^2(P_\theta)}} \right) + p_{\mathcal{N}}\left(\frac{\sqrt{\gamma_k}+|g_k|\,|\mu_{h,k}|\,\sqrt{P_\theta}}{\sqrt{\sigma_{{\rm eq},k}^2(P_\theta)}} \right) \right] \right.$$
$$\left. \frac{\sqrt{\gamma_k}\,g_k^2\,\sigma_{h,k}^2}{2\,\left[\sigma_{{\rm eq},k}(P_\theta)\right]^3} \left[p_{\mathcal{N}}\left(\frac{\sqrt{\gamma_k}+|g_k|\,|\mu_{h,k}|\,\sqrt{P_\theta}}{\sqrt{\sigma_{{\rm eq},k}^2(P_\theta)}} \right) + p_{\mathcal{N}}\left(\frac{\sqrt{\gamma_k}+|g_k|\,|\mu_{h,k}|\,\sqrt{P_\theta}}{\sqrt{\sigma_{{\rm eq},k}^2(P_\theta)}} \right) \right] \right\} \quad (45)$$

$1]/x=1$) is:

$$\left.\frac{\partial \log P(\hat{\boldsymbol{d}};P_\theta,\boldsymbol{x}_T)}{\partial P_\theta}\right|_{P_\theta=P_{\theta_0}} = \sum_{k=1}^{K} \left\{ \frac{\left(\hat{d}_k-\alpha_{0,k}^{\rm sq}\right)}{\alpha_{0,k}^{\rm sq}\left[1-\alpha_{0,k}^{\rm sq}\right]} \right.$$
$$\left. \times\,(1-2P_{e,k})\,p_{\mathcal{N}}\left(\sqrt{\frac{\gamma_k}{\sigma_{w,k}^2}}\right) \frac{\sqrt{\gamma_k}\,g_k^2\left[\mu_{h,k}^2+\sigma_{h,k}^2\right]}{\sigma_{w,k}^3} \right\} \quad (47)$$

By exploiting the definition

$$\Xi_k^{\rm sq} \triangleq \frac{(1-2P_{{\rm e},k})}{\alpha_{0,k}^{\rm sq}\left[1-\alpha_{0,k}^{\rm sq}\right]} \frac{\sqrt{\gamma_k}\left[\mu_{h,k}^2+\sigma_{h,k}^2\right]}{\sigma_{w,k}^3}\, p_{\mathcal{N}}\left(\sqrt{\frac{\gamma_k}{\sigma_{w,k}^2}}\right) \quad (48)$$

we obtain the final expression:

$$\left.\frac{\partial \log P(\hat{\boldsymbol{d}};P_\theta,\boldsymbol{x}_T)}{\partial P_\theta}\right|_{P_\theta=P_{\theta_0}} = \sum_{k=1}^{K} \left(\hat{d}_k-\alpha_{0,k}^{\rm sq}\right) \Xi_k^{\rm sq}\, g_k^2 \quad (49)$$

This concludes the proof.

APPENDIX B
DERIVATION OF THE FISHER INFORMATION

In this Appendix, we derive the $\boldsymbol{x}_T$-conditional FI expressions needed for G-Rao and G-LOD tests, respectively.

In detail, exploiting (conditional) independence of the bits received from different sensors (this applies to both RQ and SQ), we express both these quantities as:

$$I^{\rm rq}(\theta,\boldsymbol{x}_T) = \sum_{k=1}^{K} I_k^{\rm rq}(\theta,\boldsymbol{x}_T)\,, \quad (50)$$

$$I^{\rm sq}(P_\theta,\boldsymbol{x}_T) = \sum_{k=1}^{K} I_k(P_\theta,\boldsymbol{x}_T)\,, \quad (51)$$

where we have denoted with $I_k^{\rm rq}(\theta,\boldsymbol{x}_T)$ (resp. $I_k^{\rm sq}(P_\theta,\boldsymbol{x}_T)$) the contribution of kth sensor to the FI, that is $I_k^{\rm rq}(\theta,\boldsymbol{x}_T,) = \mathbb{E}\left\{(\partial \ln[P(\hat{b}_k|\boldsymbol{x}_T,\theta)]/\partial\theta)^2\right\}$ (resp. $I_k^{\rm sq}(P_\theta,\boldsymbol{x}_T) = \mathbb{E}\left\{(\partial \ln[P(\hat{d}_k|\boldsymbol{x}_T,P_\theta)]/\partial P_\theta)^2\right\}$). Then, the substitution $\theta \to \theta_0$ in $I^{\rm rq}(\theta,\boldsymbol{x}_T)$ (and exploiting Eq. (44)) provides:

$$I^{\rm rq}(\theta_0,\boldsymbol{x}_T) = \sum_{k=1}^{K} \mathbb{E}\left\{ \left[\left(\hat{b}_k-\alpha_{0,k}^{\rm rq}\right)\right]^2 \right\} (\Xi_k^{\rm rq})^2\, g_k^2 \quad (52)$$

$$= \sum_{k=1}^{K} \alpha_{0,k}^{\rm rq}\left[1-\alpha_{0,k}^{\rm rq}\right] (\Xi_k^{\rm rq})^2\, g_k^2 \quad (53)$$

and a similar expression holds for G-LOD case (exploiting Eq. (49)), that is:

$$I^{\rm sq}(P_{\theta_0},\boldsymbol{x}_T) = \sum_{k=1}^{K} \mathbb{E}\left\{ \left[\left(\hat{d}_k-\alpha_{0,k}^{\rm sq}\right)\right]^2 \right\} (\Xi_k^{\rm sq})^2\, g_k^4 \quad (54)$$

$$= \sum_{k=1}^{K} \alpha_{0,k}^{\rm sq}\left[1-\alpha_{0,k}^{\rm sq}\right] (\Xi_k^{\rm sq})^2\, g_k^4 \quad (55)$$

By using the definitions $\psi_{0,k}^{\rm rq} \triangleq \alpha_{0,k}^{\rm sq}\left(1-\alpha_{0,k}^{\rm sq}\right)(\Xi_k^{\rm rq})^2$ and $\psi_{0,k}^{\rm sq} \triangleq \alpha_{0,k}^{\rm sq}\left(1-\alpha_{0,k}^{\rm sq}\right)(\Xi_k^{\rm sq})^2$, in conjunction with Eq. (50), we obtain the (conditional) final FI results in Eqs. (16) and (20), respectively.

REFERENCES

[1] ITU-T Rec. Y.2060 (06/2012), "Overview of the Internet of Things (IoT)," Jun. 2012.

[2] M. A. Al-Jarrah, M. A. Yaseen, A. Al-Dweik, O. A. Dobre, and E. Alsusa, "Decision fusion for IoT-based wireless sensor networks," *IEEE Internet Things J.*, vol. 7, no. 2, pp. 1313–1326, 2019.

[3] P. K. Varshney, *Distributed Detection and Data Fusion*, 1st ed. Springer-Verlag New York, Inc., 1996.

[4] D. Ciuonzo and P. Salvo Rossi, Eds., *Data Fusion in Wireless Sensor Networks: A statistical signal processing perspective*, ser. Control, Robotics & Sensors. Institution of Engineering and Technology (IET), 2019.

[5] Z. Chen and Y. Zhang, "Providing spectrum information service using TV white space via distributed detection system," *IEEE Trans. Veh. Technol.*, vol. 68, no. 8, pp. 7655–7667, 2019.

[6] H. Zayyani, F. Haddadi, and M. Korki, "One-bit spectrum sensing in cognitive radio sensor networks," *Springer Circuits, Systems, and Signal Processing*, vol. 39, no. 5, pp. 2730–2743, 2020.

[7] D. Ciuonzo and P. Salvo Rossi, "Distributed detection of a non-cooperative target via generalized locally-optimum approaches," *Information Fusion*, vol. 36, pp. 261–274, 2017.

[8] H. Zayyani, F. Haddadi, and M. M. Korki, "Double detector for sparse signal detection from one-bit compressed sensing measurements," *IEEE Signal Process. Lett.*, vol. 23, no. 11, pp. 1637–1641, 2016.

[9] C. Li, Y. He, X. Wang, G. Li, and P. K. Varshney, "Distributed detection of sparse stochastic signals via fusion of 1-bit local likelihood ratios," *IEEE Signal Process. Lett.*, vol. 26, no. 12, pp. 1738–1742, 2019.

[10] C. Li, G. Li, and P. K. Varshney, "Distributed detection of sparse stochastic signals with 1-bit data in tree-structured sensor networks," *IEEE Trans. Signal Process.*, 2020.

[11] I. Y. Hoballah and P. K. Varshney, "Distributed Bayesian signal detection," *IEEE Trans. Inf. Theory*, vol. 35, no. 5, pp. 995–1000, 1989.

[12] A. R. Reibman and L. W. Nolte, "Optimal detection and performance of distributed sensor systems," *IEEE Trans. Aerosp. Electron. Syst.*, no. 1, pp. 24–30, 1987.

[13] J. N. Tsitsiklis, "Decentralized detection," *Advances in Statistical Signal Processing*, vol. 2, no. 2, pp. 297–344, 1993.

[14] R. Viswanathan and P. K. Varshney, "Distributed detection with multiple sensors - Part I: Fundamentals," *Proceedings of IEEE*, vol. 85, no. 1, pp. 54–63, Jan. 1997.

[15] D. Ciuonzo, P. Salvo Rossi, and P. Willett, "Generalized Rao test for decentralized detection of an uncooperative target," *IEEE Signal Process. Lett.*, 2017.

[16] J. Fang, Y. Liu, H. Li, and S. Li, "One-bit quantizer design for multisensor GLRT fusion," *IEEE Signal Process. Lett.*, vol. 20, no. 3, pp. 257–260, Mar. 2013.
[17] S. Laitrakun, "Decision fusion for composite hypothesis testing in wireless sensor networks over a shared and noisy collision channel," *Int. J. Distrib. Sens. Netw.*, vol. 16, no. 7, p. 1550147720940204, 2020.
[18] D. Ciuonzo and P. Salvo Rossi, "Decision fusion with unknown sensor detection probability," *IEEE Signal Process. Lett.*, vol. 21, no. 2, pp. 208–212, Feb. 2014.
[19] F. H. Bijarbooneh, W. Du, E. C.-H. Ngai, X. Fu, and J. Liu, "Cloud-assisted data fusion and sensor selection for Internet of Things," *IEEE Internet Things J.*, vol. 3, no. 3, pp. 257–268, 2015.
[20] S. M. Kay, *Fundamentals of Statistical Signal Processing, Volume 2: Detection Theory*. Prentice Hall PTR, Jan. 1998.
[21] R. Niu and P. K. Varshney, "Joint detection and localization in sensor networks based on local decisions," in *40th Asilomar Conference on Signals, Systems and Computers*, 2006, pp. 525–529.
[22] A. Shoari and A. Seyedi, "Detection of a non-cooperative transmitter in Rayleigh fading with binary observations," in *IEEE Military Communications Conference (MILCOM)*, 2012, pp. 1–5.
[23] D. Ciuonzo and P. Salvo Rossi, "Quantizer design for generalized locally optimum detectors in wireless sensor networks," *IEEE Wireless Commun. Lett.*, vol. 7, no. 2, pp. 162–165, 2018.
[24] D. Ciuonzo and P. Salvo Rossi, "Distributed detection of a non-cooperative target with multiplicative fading," in *International Symposium on Signal Processing and Intelligent Recognition Systems (SIRS)*. Springer, 2019, pp. 263–275.
[25] J. Zhu, X. Lin, R. S. Blum, and Y. Gu, "Parameter estimation from quantized observations in multiplicative noise environments," *IEEE Trans. Signal Process.*, vol. 63, no. 15, pp. 4037–4050, 2015.
[26] X. Wang, G. Li, and P. K. Varshney, "Distributed detection of weak signals from one-bit measurements under observation model uncertainties," *IEEE Signal Process. Lett.*, vol. 26, no. 3, pp. 415–419, 2019.
[27] B. Martinez, F. Adelantado, A. Bartoli, and X. Vilajosana, "Exploring the performance boundaries of NB-IoT," *IEEE Internet Things J.*, vol. 6, no. 3, pp. 5702–5712, 2019.
[28] R. D. Davies, "Hypothesis testing when a nuisance parameter is present only under the alternative," *Biometrika*, vol. 74, no. 1, pp. 33–43, 1987.
[29] F. Gao, L. Guo, H. Li, and J. Fang, "One-bit quantization and distributed detection with an unknown scale parameter," *Algorithms*, vol. 8, no. 3, pp. 621–631, 2015.
[30] D. Ciuonzo, G. Romano, and P. Salvo Rossi, "Channel-aware decision fusion in distributed MIMO wireless sensor networks: Decode-and-fuse vs. decode-then-fuse," *IEEE Trans. Wireless Commun.*, vol. 11, no. 8, pp. 2976–2985, Aug. 2012.
[31] D. Ciuonzo, G. Papa, G. Romano, P. Salvo Rossi, and P. Willett, "One-bit decentralized detection with a Rao test for multisensor fusion," *IEEE Signal Process. Lett.*, vol. 20, no. 9, pp. 861–864, 2013.
[32] H. C. Papadopoulos, G. W. Wornell, and A. V. Oppenheim, "Sequential signal encoding from noisy measurements using quantizers with dynamic bias control," *IEEE Trans. Inf. Theory*, vol. 47, no. 3, pp. 978–1002, Mar. 2001.
[33] D. Rousseau, G. V. Anand, and F. Chapeau-Blondeau, "Nonlinear estimation from quantized signals: Quantizer optimization and stochastic resonance," in *Proc. 3rd Int. Symp. Physics in Signal and Image Processing*, 2003, pp. 89–92.
[34] A. Ribeiro and G. B. Giannakis, "Bandwidth-constrained distributed estimation for wireless sensor networks - Part I: Gaussian case," *IEEE Trans. Signal Process.*, vol. 54, no. 3, pp. 1131–1143, Mar. 2006.
[35] X. Cheng, D. Ciuonzo, P. Salvo Rossi, X. Wang, and L. Shi, "Multi-bit decentralized detection of a non-cooperative moving target through a generalized Rao test," in *IEEE 11th Sensor Array and Multichannel Signal Processing Workshop (SAM)*, 2020, pp. 1–5.
[36] P.-Y. Chen, S.-M. Cheng, and K.-C. Chen, "Information fusion to defend intentional attack in internet of things," *IEEE Internet Things J.*, vol. 1, no. 4, pp. 337–348, 2014.
[37] N. Biswas, P. Ray, and P. K. Varshney, "Distributed detection over channels with memory," *IEEE Signal Process. Lett.*, vol. 22, no. 12, pp. 2494–2498, 2015.
[38] J. Fang, X. Li, H. Li, and L. Huang, "Precoding for decentralized detection of unknown deterministic signals," *IEEE Trans. Aerosp. Elect. Syst.*, vol. 50, no. 3, pp. 2116–2128, July 2014.

Domenico Ciuonzo (SM'16) is an Assistant Professor at University of Napoli Federico II. He holds a Ph.D. in Electronic Engineering from the University of Campania, Italy. Since '11, he has been holding several visiting researcher appointments. Since '14, he has been (Area) Editor of several IEEE journals. He is the recipient of Best Paper awards from IEEE ICCCS ('19) and COMPUTER NETWORKS ('20), the Exceptional Service award from IEEE AESS ('19), and the Early-Career Technical Achievement award from IEEE SENSORS COUNCIL for sensor networks/systems ('20). His research interests include data fusion, wireless sensor networks, the Internet of Things and machine learning.

Pierluigi Salvo Rossi (SM'11) was born in Naples, Italy, in 1977. He received the Dr.Eng. degree (*summa cum laude*) in telecommunications engineering and the Ph.D. degree in computer engineering from the University of Naples "Federico II", Italy, in 2002 and 2005, respectively. He held visiting appointments at Drexel University, USA; Lund University, Sweden; Norwegian University of Science and Technology (NTNU), Norway; and Uppsala University, Sweden. From 2005 to 2008, he held postdoctoral positions at the University of Naples "Federico II", Italy; Second University of Naples, Italy; and NTNU, Norway. He was an Assistant Professor (2008--2014, tenured in 2011) at the Second University of Naples, Italy. He was an Associate Professor (2014--2016) and a Full Professor (2016-2017) at NTNU, Norway. He was a Principal Engineer (2017--2019) with Kongsberg Digital AS, Norway. Since 2019, he is a Full Professor with the Dept. Electronic Systems, NTNU, Norway, and the Director of IoT@NTNU. His research interests fall within the areas of communication theory, data fusion, machine learning, and signal processing. He is Executive Editor for the IEEE COMMUNICATIONS LETTERS; Area Editor for the IEEE OPEN JOURNAL OF THE COMMUNICATIONS SOCIETY; Associate Editor for the IEEE TRANSACTIONS ON SIGNAL AND INFORMATION PROCESSING OVER NETWORKS. He was Associate Editor of the IEEE TRANSACTIONS ON WIRELESS COMMUNICATIONS; Senior Editor and Associate Editor of the IEEE COMMUNICATIONS LETTERS. He was awarded as an Exemplary Senior Editor of the IEEE COMMUNICATIONS LETTERS in 2018.

Pramod Varshney (LF'18) Pramod K. Varshney received the B.S. degree in electrical engineering and computer science (with highest Honors), and the M.S. and Ph.D. degrees in electrical engineering from the University of Illinois at Urbana-Champaign, USA, in 1972, 1974, and 1976 respectively. Since 1976, he has been with Syracuse University, Syracuse, NY, USA, where he is currently a Distinguished Professor of Electrical Engineering and Computer Science and the Director of CASE: Center for Advanced Systems and Engineering. He has published over 530 conference papers and 310 journal papers. During his career, he has supervised 62 doctoral dissertations. He is a member of Tau Beta Pi and received the 1981 ASEE Dow Outstanding Young Faculty Award. He was elected to the grade of Fellow of the IEEE in 1997 for his contributions in the area of distributed detection and data fusion. In 2000, he received the Third Millennium Medal from the IEEE and Chancellor's Citation for exceptional academic achievement at Syracuse University. He received the IEEE 2012 Judith A. Resnik Award, Doctor of Engineering degree honoris causa from Drexel University in 2014, the ECE Distinguished Alumni Award from the University of Illinois in 2015 and ISIF's Yaakov Bar-Shalom Award for a Lifetime of Excellence in Information Fusion in 2018. He is on the Editorial Board of the Journal on Advances in Information Fusion and has served on the editorial boards of IEEE TRANSACTIONS OF SIGNAL PROCESSING as well as IEEE SIGNAL PROCESSING MAGAZINE among others. He was the President of International Society of Information Fusion during 2001.